Biomechanics of predator prey arms race in lion, zebra, cheetah and impala

A.M. Wilson[1], T.Y. Hubel[1], S. Wilshin[1], J.C. Lowe[1], M. Lorenc[1] O.P. Dewhirst[1], H.L.A. Bartlam-Brooks[1], R. Diack[1], E. Bennitt[2], K.A. Golabek[3], R. Woledge[1†], J.W. McNutt[3], N.A. Curtin[1] & T. West[1]

[1]Structure & Motion Lab, Royal Veterinary College, University of London, Hatfield, UK. [2]Okavango Research Institute, University of Botswana, Maun, Botswana.[3]Botswana Predator Conservation Trust, Private Bag 13, Maun, Botswana. †Deceased.

The fastest and most manoeuvrable terrestrial animals are found in savannah habitats, where predators chase and capture running prey. Hunt outcome and success rate are critical to survival, so both predator and prey should evolve to be faster and/or more manoeuvrable. We compare locomotor characteristics in two pursuit predator-prey pairs, lion-zebra and cheetah-impala, in their natural savannah habitat in Botswana. We show that although cheetah and impala were universally more athletic than lion and zebra in terms of speed, acceleration and turning, within each predator-prey pair, the predators had 20% higher muscle fibre power than prey, 37% greater acceleration and 72% greater deceleration capacity than their prey. We simulated hunt dynamics with these data and showed that hunts at lower speeds enable prey to use their maximum manoeuvring performance and favour prey survival, and that the predator needs to be more athletic than its prey to sustain viable success rate.

In a chase, the prey animal can select its speed and the timing of acceleration/deceleration and turns, whilst a predator in pursuit must predict or respond to prey trajectory to enable interception and capture[1-3]. The prey should make its movements unpredictable to the predator while generally using tactics that minimise the chance the predator has of catching it[4]. So whilst the optimum avoidance strategy might be, for instance, to perform a maximum-rate turn away from the predator, using this strategy consistently would enable the predator to pre-empt that manoeuvre[5]. If a dominant evolutionary pressure on the locomotor system is predation success/evasion, then predator and associated prey should display similar high levels of athleticism[6-9] distinguished by the specific adaptations necessary to enable capture (in predators) or evade capture (in prey)[10]. We hypothesise that predators are consistently more athletic than their prey so they can manoeuvre and change speed to respond to the unpredictable tactics of the prey animal.

We studied two predator-prey pairs found on the southern African savannah where a simple high speed manoeuvring pursuit in open terrain is a commonly-used hunting technique: cheetah, *Acinonyx jubatus* (C) and impala, *Aepyceros melampus* (I)[11], which are similar in size (50-70 *vs* 50-60 kg, Methods), and the substantially larger lion, *Panthera leo* (L) and zebra, *Equus quagga* (Z)[12] (120-240 *vs* 320 kg) (Fig. 1a-d,f).

We evaluate five metrics. The first is locomotor muscle maximum power output and contraction speed, which is assumed critical for speed, acceleration and turning

1

performance[13,14]. The second metric is animal acceleration and deceleration (in the direction of travel). This combines muscle power and volume with factors including grip, body shape[15] and the anatomical arrangement of muscles[16]. Third, the highest speed commonly used by each species and the actual top speed recorded[9]. Fourth, animal turning performance (centripetal acceleration and heading rate) which can be limited by grip[17], leg strength[18] and muscle power[19,20]. Finally, stride frequency, because there is one opportunity per stride for the legs to apply impulses to change speed and direction in a hunt[21].

Locomotion data were collected from free-living wild animals undertaking high speed runs in northern Botswana using our own design of Global Positioning System and Inertial Measurement Unit collars[9] (GPS-IMU, Methods, Fig. 1, Extended Data Fig. 1a). We collected velocity and acceleration for each of 23,871 strides, 520 runs from five cheetah, 22,491 strides, 515 runs from seven impala, 111,110 strides, 2726 runs from nine lions and 64,952 strides, 1801 runs from seven zebra (Extended Data Fig. 1f). Muscle biopsies were collected from *biceps femoris*, a major propulsive muscle in the hind leg (Methods).

Muscle fibre power in predator and prey

Muscle biopsies were skinned, placed in a trehalose-glycerol mixture, frozen in liquid nitrogen in the field and transported to the UK. Peak power, velocity and stress at peak power and maximum isometric stress were determined at 25°C for single skinned fibres (Fig. 2a-f). Maximum power and associated velocity and stress were then calculated (Methods).

Complete measurements were made on 37 individual skinned fibres from six cheetah, 30 fibres from five impala, 50 fibres from eight lions and 57 fibres from eight zebra. There was a distinct subpopulation of 'low performance' fibres (twelve zebra, eight lion, three cheetah and three impala; Fig. 2c) with a velocity at peak power that was below 1.35 lengths s^{-1} and a lower peak power (Extended Data Fig. 2f) which were either myosin heavy chain (MHC) type-I (11 of 19 fibres tested) or type-II (8 fibres) (Methods).

Linear mixed-effects models were fitted for peak power, velocity and stress at peak power and isometric stress with a factor distinguishing predator and prey, including the interaction of this factor with a categorical variable called 'fibre performance classification'. Within the factor distinguishing predator and prey, we nested a random effect by subject and fibre. The residuals of this model exhibited heteroscedasticity and so the variance of the error term was allowed to vary by subject and 'performance classification'. Power in the high performance fibres was 20% greater in the predator group than in the prey group (delta = 20.0Wkg^{-1}, z=-3.46, p=0.001). The difference was similar in both pairings but the effect was only significant in the lion-zebra pairing (effect size 20.0Wkg^{-1}, 20%, z=2.56, p=0.039), cheetah-impala effect of 18.9Wkg^{-1}, 19%, z=2.04, p=0.15. The peak specific powers were very similar in the two predator species and lower but very similar in the two prey species (high performing fibres mean power ± standard error Wkg^{-1}; C – 106.7 ± 4.6, L – 108.1 ± 4.2; I – 88.3 ± 5.2, Z – 88.4 ± 4.1).

No significant differences between predators and prey were detected for velocity at peak power (effect size 0.096 lengths s^{-1}, z=-1.77, p=0.15) or stress at peak power (7.2 kPa, z=-2.05, p=0.075) for high performance fibres. Isometric stress was higher in predators (33.4kPa, z=-2.87, p=0.008).

2

The values reported here are comparable to data for wild rabbit skinned fibres at 25°C[22], but are high compared with published values for skinned fibres from large animals[23,24]. Muscle power is highly temperature-dependent[25] and a temperature coefficient (Q_{10}; ratiometric increase in rate with a temperature increase of 10 degrees) of 2.3 is appropriate[26] which predicts *in vivo* muscle power (all fibres, Extended Data Fig. 2i) of 232 (prey) and 292 (predators) Wkg^{-1} at body temperature of 38°C.

Slower myosins and muscle fibres are inherently more economical[23,25,27] so slower fibres confer advantages[25], with the fast *vs* slow distribution reflecting the opposing pressures of predation (avoidance) on one side and food/water supply, ranging distance and environmental conditions on the other[25,28]. This may partly explain why the prey species have lower power muscle fibres[25]. Hence the muscle of desert specialists at risk of dehydration/starvation[29] such as camel, vicuna and Arabian Oryx would be predicted to be biased towards economy[25]. Selection pressure for greater performance or economy could change fibre type distributions or muscle characteristics within a few generations - much more rapid than for changes in myosin contractile speed.

Speed and acceleration of free ranging predators and prey

Stride timing and hence frequency was derived from collar acceleration data[9]. Stride speed and accelerations were averaged over each stride; change in speed is difference in speed between two consecutive strides, work per stride is the change in mass-specific net horizontal kinetic energy and power per stride is the work per stride divided by stride duration. Change in heading is the angle between two consecutive stride velocity vectors[9].

Differences in the frequency of maximum effort manoeuvring between predators and prey (since predators hunt often and prey are rarely hunted) would manifest in different tails for the distributions of accelerations for each species. The predator species will have relatively heavy tails, i.e. higher kurtosis as more of their observed behaviours are associated with rapid accelerations, while the more sedentary (or at least steadily moving) prey have fewer such observations. Steady-state strides were removed by thresholding on acceleration with the threshold determined for each species by the kurtosis of these distributions resulting in a similar distribution for all species. (Methods, Extended Data Fig. 3a,b). Qualitatively the distributions for predators and for prey are similar and the 98% percentile approximates to the limit in a reasonably consistent manner across runs of all lengths and tortuosity (Extended Data Fig 4).

Stride parameters were grouped into non-uniform speed bins with 400 data points in each and the 98th percentile of value determined for each bin (except for stride frequency where data were further subgrouped on acceleration performance and a linear regression performed on each subgroup (Methods)). The uppermost bin with fewer than 400 data points was ignored. The 98th percentile was chosen to account for different numbers of strides in different species and to exclude occasional extreme values[9] (Extended Data Fig. 5,6). The cheetah-impala pairing were more athletic than the zebra-lion pairing in every metric (Extended Data Fig. 7).

Predator and prey were compared using a linear model (Methods) and test statistics computed under the null that predator and prey are drawn from the same distribution, except for stride frequency where due to species differences predator and prey pairs were compared individually. The ratio of the maximum observed performance for cheetah-impala then lion-zebra, along with the results of the test comparing predator and prey across species, are as follows: predators were 50% and 24% better in acceleration (z=3.15, p=0.0016), 73% and 70% better in deceleration (z=-6.61, p<0.0001) 100% and 89% more powerful in acceleration (z=3.87, p=0.0001) and 100% and 122% more powerful in deceleration (z=-8.07, p<0.0001). Stride frequency was higher in cheetah than in impala (z=3.69, p<0.001) and lower in lion than zebra (z=-2.31, p=0.041). Stride frequency at 8ms^{-1} was 6% higher in acceleration (p=0.0018) and 5% higher in deceleration (p<0.001) than in steady speed locomotion, post-hoc tests on linear model.

The 98th percentile of speed was C - 19.9, I - 13.8, L - 13.9 and Z - 10.6 ms^{-1} which is 84, 78, 67 and 77% of the maximum achieved by three individuals which were C - 23.8, I - 17.7, L - 20.6 and Z - 13.8ms^{-1}. So predators were faster than their prey and all species rarely approached their maximum recorded speed (Extended Data Fig. 5).

Turning performance of free ranging predators and prey

In turning, predators were only slightly superior to prey (z=2.93, p=0.0034): cheetah-impala 15%, lion-zebra 10% (Fig. 3k-n). Turning does not require a change in body kinetic energy, but a centripetal acceleration of 13ms^{-2} results in a 66% increase in effective weight[18] and the limbs must shorten and extend in the presence of these higher axial forces. This length change can be delivered by passive elastic structures within the limb[30,31] but any associated muscles must deliver higher forces at that contraction velocity (equating to a higher power requirement)[19,20]. Reduced centripetal acceleration at high speed would indicate a muscle limit rather than a grip limit for that activity[17,19] but we found no evidence for such a limit[18] at these submaximal speeds.

Figure 3n summarises the capacity for maximum acceleration in any direction, relative to the track of the animal. It shows that these predators outperform their prey most markedly in deceleration (bottom of plot) and less so in forward acceleration (top of plot) and turning (sides of plot). No species showed highest levels of tangential and centripetal acceleration in the same stride; the lines are elliptical, which supports a grip type limit (as horizontal accelerations should vector sum to a limit value). Forward acceleration performance was maintained by all four species at the fastest speeds commonly used (Fig. 3e,j). Power requirements for forward acceleration increase with speed (Fig. 3c,h, Extended Data Fig. 5) since power is the product of speed and acceleration, and if acceleration was reduced at highest speeds this would indicate a potential power constraint[15]. A diminution in manoeuvrability would result in an animal's trajectory being more predictable, which would be disadvantageous for both predator and prey.

Discussion of species differences in experimental data

Much of the difference observed between predator and prey could be attributed to predators having proportionally more muscle and/or higher muscle power (Fig. 2d), but that does not

4

provide an explanation for the large differences observed between lion and cheetah and between zebra and impala (Extended Data Fig. 7). Hind limb muscle fraction of total body mass is fairly consistent across species: 17.5 - 19.8% (Extended Data Table 1), so muscle peak power should define whole animal acceleration capacity at moderate to high speed[9,13,15]. Athletic wild animals are, however, likely to be proportionally more muscular than the mostly sedentary domesticated animals contributing to Extended Data Table 1 and spinal, trunk and forelimb muscle will also contribute to acceleration. The predicted *in vivo* muscle powers of 232 - 292Wkg^{-1} are concomitant with the upper but not the lower limit of observed whole animal powers of 30-120Wkg^{-1} (Fig. 3e).

Carnivores hunt with empty stomachs, whilst prey carry the mass of the rumen (impala) or hind gut (zebra) contents which will impinge on any performance that is dependent on muscle power or strength (as would pregnancy). The differences within the predator and within the prey species may reflect that the muscles are arranged for different roles, e.g. for economical walking *vs* for acceleration and hunting/fighting[25,32,33], but without contextual anatomical data that is only speculation and the differences are too large to simply be attributed to scaling due to animal size (Extended Data Table 2a). Foot design and grip may also play a role[34]. Behavioural factors cannot be ruled out but Extended Data Figs. 5,6 reassure that the highest values were captured.

Capture–evasion model description and predictions

A pursuit predator uses a combination of stealth and speed to get close to its prey[12] and then the prey evades capture by manoeuvring[1,4] whilst the predator attempts to intercept it. The interaction has been approached analytically or numerically for continuous processes[35,36] (e.g. air combat manoeuvring) but modelling the probability that the predator and prey arrive at the same location becomes increasingly complex to solve when treated as a discrete process.

In our model, predator and prey were able to accelerate in any direction up to their experimentally derived maximum in each stride, so they could go anywhere on the boundary of an approximately elliptical area which grew with the subsequent stride (Fig. 4a-c). The predator responded to the prey acceleration in the preceding stride and we modelled initial conditions where the predator could catch its prey within two strides. The acceleration limits for each species and direction (impulses per stride) were the observed 98% centripetal, positive and negative tangential acceleration divided by the stride frequency at that speed (Fig. 3b,e,g,j). The elliptical area precluded simultaneous maximal centripetal and tangential accelerations (Fig. 3n). At higher speeds, acceleration and hence manoeuvring were curtailed as the applied impulses could not cause the animal to exceed the 98% maximum speed observed for each species.

For the prey, the accelerations at the start of the first and second stride were the possible accelerations up to maximum (Extended Data Table 2b) in any direction. The predator had zero acceleration in the first stride so its initial velocity determined its subsequent position and it could accelerate in any direction in the second stride (reacting to the previous prey acceleration). The area reached by the predator was augmented by a semi-circular region of half body length in front of the predator to account for the physical size of the predator. We

define capture probability as the fraction of the elliptical area for the prey that is covered by the predator's elliptical area after two strides.

We plotted the feasible range of initial prey speeds and predator-prey spacings for capture after two strides (Fig. 4d, Extended Data Fig. 8) and then optimised the initial predator speed for each condition to maximise the overlap in position between the predator and the prey after two strides. The predator-prey spacing at the beginning of the simulation represents less than a stride length in all cases (model code, Python, in Suppl Information).

The model shows that the prey should avoid the predator by turning (lateral acceleration) rather than attempting to increase separation by travelling as fast as possible (Fig. 4d). If the prey is moving fast and the predator is close (bottom left region of Fig. 4d) its best option requires rapid deceleration and turning, whilst only turning becomes more beneficial if the predator is further away (and hence closing at higher relative speed, bottom right region of Fig. 4d). High prey speeds result in high capture probabilities (Fig. 4f) because the prey cannot accelerate forwards with or without turning, making its tactics highly predictable (captured by optimisation of predator speed for overlap), whilst a slow moving prey (left side of Fig. 4e,f) has a wider variety of escape options and hence is less predictable. Predator and prey indeed use moderate speeds (Fig. 4e,f).

The predator has the highest chance of success if it is travelling only slightly faster than the prey, which enables it to reach many of the locations the prey can move to over a broad range of starting speeds (the objective function for the optimisation, relative capture area, is very flat in this region) with its advantage increasing with higher prey speeds. This is reflected in observed actual predator speeds (Fig. 4e,f).

Figure 5 shows that all species often execute a constant speed turn but it is rare for either of the herbivore species to accelerate or decelerate whilst the predators (especially lions) often undertake deceleration strides, either in isolation or in combination with a turn. The preferred accelerations fit with the prey using optimum escape strategies predicted by the non-overlapping areas in Fig. 4d and tactics where they have performance similar to the predators (turning) rather than those where they are outperformed – tangential acceleration and deceleration. With the same lateral acceleration a prey that is moving more slowly than a converging faster-moving predator will have an advantageously tighter turn, since radius is equal to v^2/lateral acceleration. Commonly observed predator decelerations are concomitant with a faster-moving closing predator. More than one repetition of the modelled two-stride scenario can occur within a single pursuit[9] –and the overlap-derived success rates are similar to those observed for animals hunting in the wild[9,12,37].

Effect of predator and prey athleticism on hunting success rate

We adjusted the acceleration capacity of the predator or prey and reran the simulation to obtain capture probabilities for animals of greater or lesser athleticism. Unsurprisingly, increased predator performance is beneficial, reducing the number of hunts needed to capture prey (Fig. 4g,h). Due to the power relationship underlying the figure, curves steepen when the predator is below 0.8 of its actual performance (Fig. 4h), which would tend towards an unsustainably low success rate (ignoring other determinants of hunt outcome). Such a

diminution could be the result of injury or aging with greatest consequences for solitary animals. The data also provide insight into preferred prey and hunting style: the predicted low success rate for lions hunting impala (Fig. 4g,h) is supported by the observation that they capture impala opportunistically rather than in an open pursuit. African wild dogs hunt impala[37] but are less athletic than cheetah[37]. Applying the model to a single African wild dog hunting an impala[37] predicts a success rate of 8.2% which is lower than the actual success rate of 15.5%[37] which would concur with them using opportunistic captures rather than one on one hunts[37].

Conclusions

The study shows that overall, the athletic capabilities of the two pursuit predators closely match their respective common prey, delivering a sustainable success/survival rate and reflecting an evolutionary arms race[6,7]. The predators have higher muscle power, are faster and have a greater capacity to accelerate and decelerate than their prey. The prey can match their predator's locomotor capabilities most closely through turning manoeuvrability, affording them a critical escape space. In evolutionary terms, there may be scope for further development of performance, for instance through increasing muscle power, but this specialisation may be at the cost of locomotor economy, musculosketal robustness, or other ecologically relevant factors like prey capture, fighting or the capacity to adapt to a changing world.

References

1   Howland, H. C. Optimal strategies for predator avoidance: The relative importance of speed and manoeuvrability. *J. Theor. Biol.* **47**, 333-350, doi:10.1016/0022-5193(74)90202-1 (1974).
2   Moore, T. Y. & Biewener, A. A. Outrun or outmaneuver: Predator–prey interactions as a model system for integrating biomechanical studies in a broader ecological and evolutionary context. *Integr. Comp. Biol.*, icv074 (2015).
3   Combes, S., Salcedo, M., Pandit, M. & Iwasaki, J. Capture success and efficiency of dragonflies pursuing different types of prey. *Integr. Comp. Biol.* **53**, 787-798 (2013).
4   Domenici, P., Booth, D., Blagburn, J. M. & Bacon, J. P. Cockroaches keep predators guessing by using preferred escape trajectories. *Curr. Biol.* **18**, 1792-1796 (2008).
5   Blagburn, J. M. & Bacon, J. P. Animal escapology II: escape trajectory case studies. *J. Exp. Biol.* **214**, 2474-2494 (2011).
6   Van Valen, L. A new evolutionary law. *Evol Theory* **1**, 1-30 (1973).
7   Benton, M. J. The Red Queen and the Court Jester: species diversity and the role of biotic and abiotic factors through time. *Science* **323**, 728-732 (2009).
8   Bro-Jørgensen, J. Evolution of sprint speed in African savannah herbivores in relation to predation. *Evolution* **67**, 3371-3376 (2013).
9   Wilson, A. M. *et al.* Locomotion dynamics of hunting in wild cheetahs. *Nature* **498**, 185-189 (2013).
10   Irschick, D. J. & Higham, T. E. *Animal athletes: an ecological and evolutionary approach.* (Oxford University Press, 2015).
11   Broekhuis, F., Cozzi, G., Valeix, M., McNutt, J. W. & Macdonald, D. W. Risk avoidance in sympatric large carnivores: reactive or predictive? *J. Anim. Ecol.* **82**, 1098-1105, doi:10.1111/1365-2656.12077 (2013).

12   Schaller, G. B. *The Serengeti Lion: A Study of Predator-prey Relations*. (University of Chicago Press, 1972).

13   Curtin, N. A., Woledge, R. C. & Aerts, P. Muscle directly meets the vast power demands in agile lizards. *Proc. R. Soc. Lond. B Biol. Sci.* **272**, 581-584 (2005).

14   Kohn, T. A. & Noakes, T. D. Lion (*Panthera leo*) and caracal (*Caracal caracal*) type IIx single muscle fibre force and power exceed that of trained humans. *J. Exp. Biol.* **216**, 960-969 (2013).

15   Williams, S. B., Tan, H., Usherwood, J. R. & Wilson, A. M. Pitch then power: limitations to acceleration in quadrupeds. *Biol. Lett.* **5**, 610-613 (2009).

16   Carrier, D. R., Gregersen, C. S. & Silverton, N. A. Dynamic gearing in running dogs. *J. Exp. Biol.* **201**, 3185-3195 (1998).

17   Tan, H. & Wilson, A. M. Grip and limb force limits to turning performance in competition horses. *Proc. R. Soc. Lond. B Biol. Sci.* **278**, 2105-2111 (2011).

18   Usherwood, J. R. & Wilson, A. M. Biomechanics: No force limit on greyhound sprint speed. *Nature* **438**, 753-754, doi:10.1038/438753a (2005).

19   Daley, M. A. Non-Steady Locomotion. *Understanding Mammalian Locomotion: Concepts and Applications,* 277-306 (Wiley & Sons, 2016).

20   Wilson, J. W. *et al.* Cheetahs, *Acinonyx jubatus*, balance turn capacity with pace when chasing prey. *Biol. Lett.* **9**, doi:10.1098/rsbl.2013.0620 (2013).

21   Jindrich, D. L., Smith, N. C., Jespers, K. & Wilson, A. M. Mechanics of cutting maneuvers by ostriches (*Struthio camelus*). *J. Exp. Biol.* **210**, 1378-1390 (2007).

22   Curtin, N. A., Diack, R. A., West, T. G., Wilson, A. M. & Woledge, R. C. Skinned fibres produce the same power and force as intact fibre bundles from muscle of wild rabbits. *J. Exp. Biol.* **218**, 2856-2863 (2015).

23   Rome, L. C., Sosnicki, A. A. & Goble, D. Maximum velocity of shortening of three fibre types from horse soleus muscle: implications for scaling with body size. *J. Physiol.* **431**, 173-185 (1990).

24   Seow, C. & Ford, L. Shortening velocity and power output of skinned muscle fibers from mammals having a 25,000-fold range of body mass. *J. Gen. Physiol.* **97**, 541-560 (1991).

25   Hill, A. V. The dimensions of animals and their muscular dynamics. *Science Progress (1933-)* **38**, 209-230 (1950).

26   West, T. G. *et al.* Power output of skinned skeletal muscle fibres from the cheetah (Acinonyx jubatus). *J. Exp. Biol.* **216**, 2974-2982 (2013).

27   Crow, M. T. & Kushmerick, M. J. Chemical energetics of slow-and fast-twitch muscles of the mouse. *J. Gen. Physiol.* **79**, 147-166 (1982).

28   Bartlam-Brooks, H. L., Bonyongo, M. C. & Harris, S. How landscape scale changes affect ecological processes in conservation areas: external factors influence land use by zebra (*Equus burchelli*) in the Okavango Delta. *Ecol. Evol.* **3**, 2795-2805 (2013).

29   Schmidt-Nielsen, K. *Desert animals. Physiological problems of heat and water*. (Clarendon Press, 1965).

30   Wilson, A. M., McGuigan, M. P., Su, A. & van den Bogert, A. J. Horses damp the spring in their step. *Nature* **414**, 895-899 (2001).

31   McGuigan, M. P. & Wilson, A. M. The effect of gait and digital flexor muscle activation on limb compliance in the forelimb of the horse *Equus caballus*. *J. Exp. Biol.* **206**, 1325-1336 (2003).

32   Pasi, B. & Carrier, D. R. Functional trade-offs in the limb muscles of dogs selected for running vs. fighting. *J. Evol. Biol.* **16**, 324-332 (2003).

33   Carrier, D. R., Anders, C. & Schilling, N. The musculoskeletal system of humans is not tuned to maximize the economy of locomotion. *PNAS* **108**, 18631-18636 (2011).

34   Wynn, M. L., Clemente, C., Nasir, A. F. A. A. & Wilson, R. S. Running faster causes disaster: trade-offs between speed, manoeuvrability and motor control when running around corners in northern quolls (Dasyurus hallucatus). *J. Exp. Biol.* **218**, 433-439 (2015).

35   Merz, A. The homicidal chauffeur. *AIAA Journal* **12**, 259-260 (1974).

36   Getz, W. & Pachter, M. Two-target pursuit-evasion differential games in the plane. *J. Optim. Theory. Appl.* **34**, 383-403 (1981).

37   Hubel, T. Y. *et al.* Energy cost and return for hunting in African wild dogs and cheetahs. *Nat. Commun.* **7**, doi:10.1038/ncomms11034 (2016).
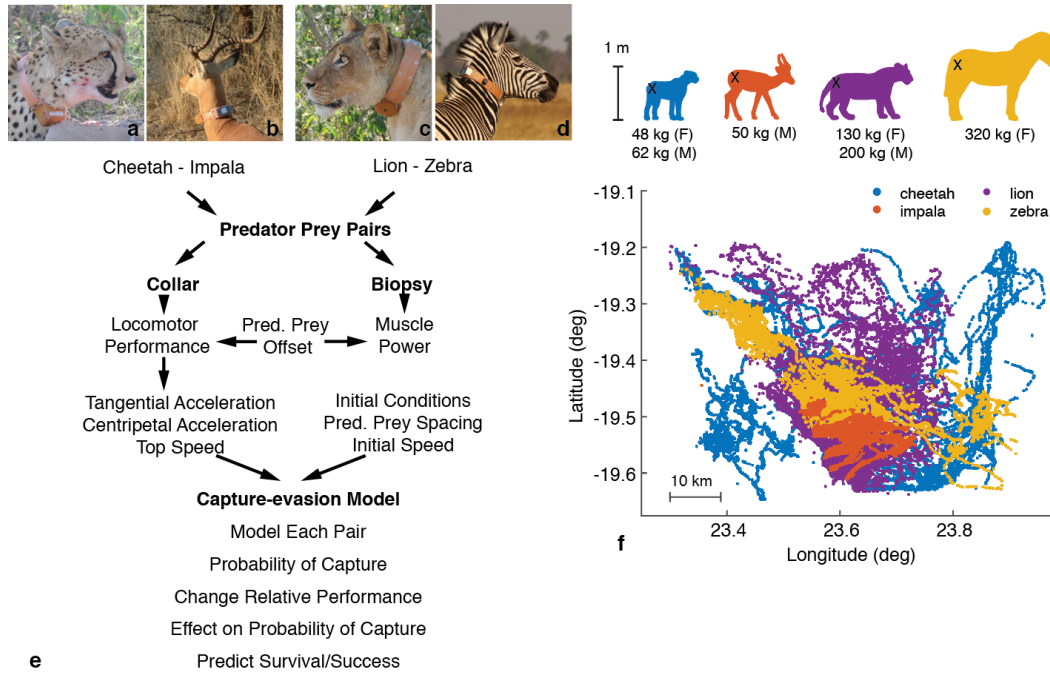
Figure 1. Overview. (a-d) The four species in the study showing collars and in **(d)** release mechanism. **(e)** flowchart summarising paper. **(f)** relative animal size and biopsy location (black cross on animal) along with collar GPS position data for the four species showing range overlap. (cheetah – blue, impala – red, lion – purple and zebra – yellow)
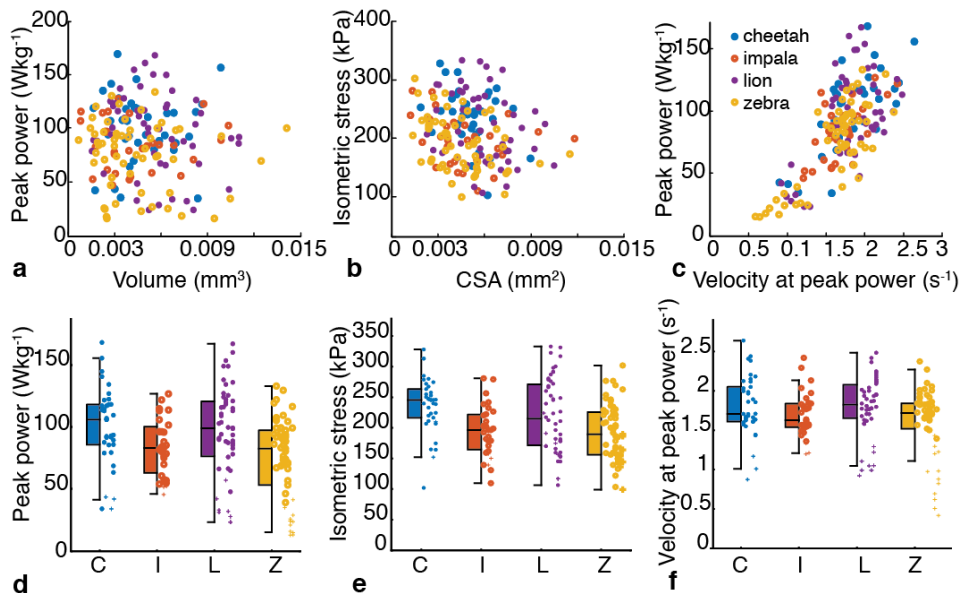

Figure 2. Muscle Contraction Mechanics. (a) Peak power *vs* volume **(b)** maximum isometric stress *vs* cross sectional area **(c)** peak power *vs* velocity at peak power, each point is a fibre, key in **(c)**. **(d-f)** box-plots showing variations in power **(d)**, isometric stress **(e)** optimal shortening velocity **(f)** across the four species, with each fibre represented and data from each individual in a separate vertical column. (Line is median, box is IQR, whiskers are 1.5*IQR). Presented data comprises 37 fibres from six cheetah, 30 fibres from five impala, 50 fibres from eight lions and 57 fibres from eight zebra.
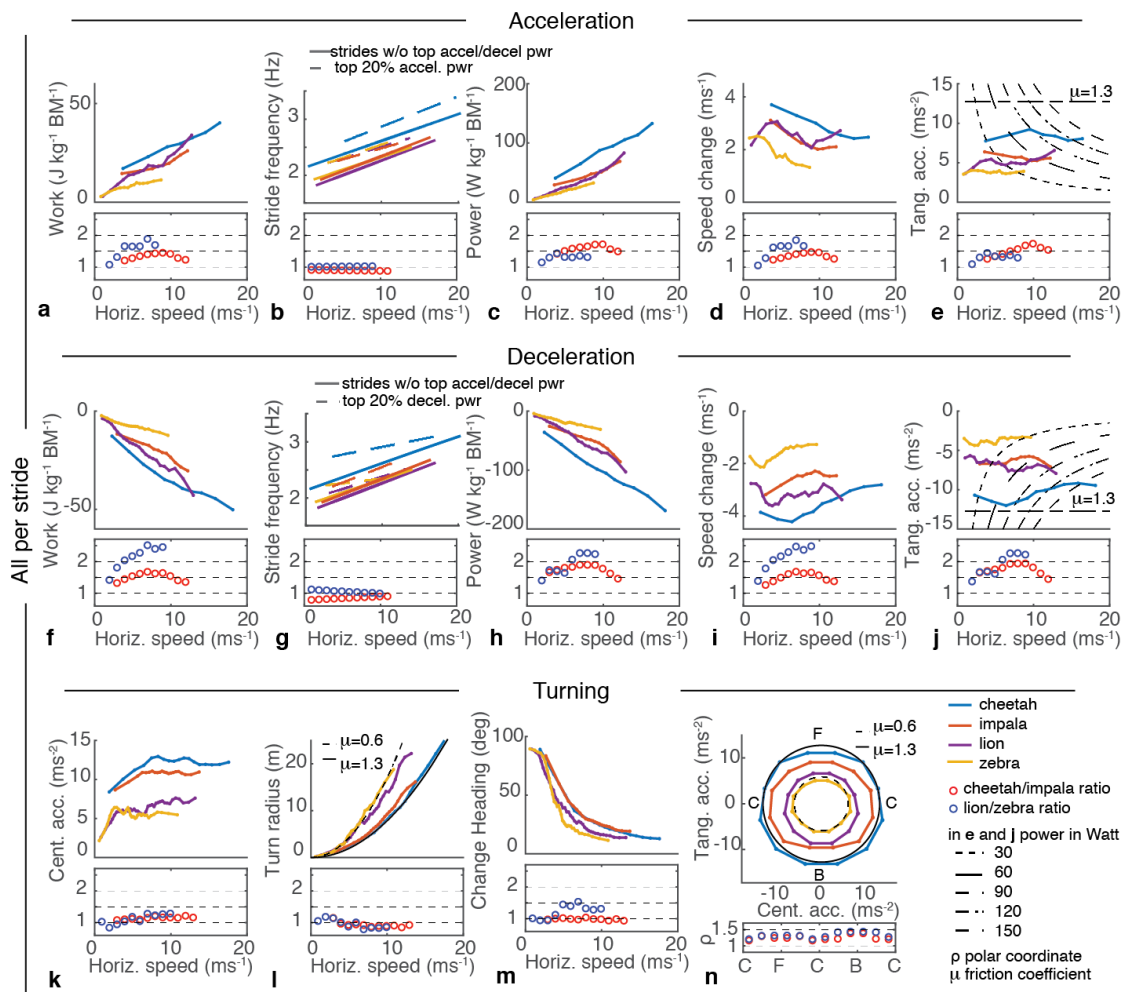
Figure 3. Locomotor performance based on stride parameters. All values are averaged per stride or represent the change over a stride and where appropriate are per kg body mass. Acceleration: **(a)** positive net work performed in each stride **(b)** stride frequency, mean of 20% highest power strides and middle 60% of power strides **(c)** stride average power **(d)** increase in speed per stride and **(e)** tangential (forward) acceleration with the curved lines representing a stride mean power of 30, 60, 90, 120, 150 Wkg⁻¹, limit line for a coefficient of friction (μ) of 1.3. Parts **(f–j)** are the same figures as **(a-e)** but for decelerating strides. Turning: **(k)** centripetal acceleration, **(l)** the relationship between speed and turn radius with limit lines for a coefficient of friction (μ) of 0.6 and 1.3, **(m)** change in heading *vs* speed in and **(n)** tangential against centripetal (lateral) acceleration with μ limits as for (l). In **(n)** F represents pure forward acceleration, B deceleration and C centripetal acceleration. In each panel there is one line per species which (except **b,g**) represents the 98th percentile for data in speed bins (each bin contains 400 data points consequently bin width varies) (cheetah – blue, impala – red, lion – purple and zebra – yellow). On the lower part of each panel, the ratio of that parameter for cheetah to impala (red circle) and lion to zebra (blue circle) is given for each speed bin, same x axis. Data set comprised 7509 strides, 520 runs from five cheetah, 8884 strides, 515 runs from seven impala, 15947 strides, 2726 runs from nine lions and 14089 strides, 1801 runs from seven zebra.
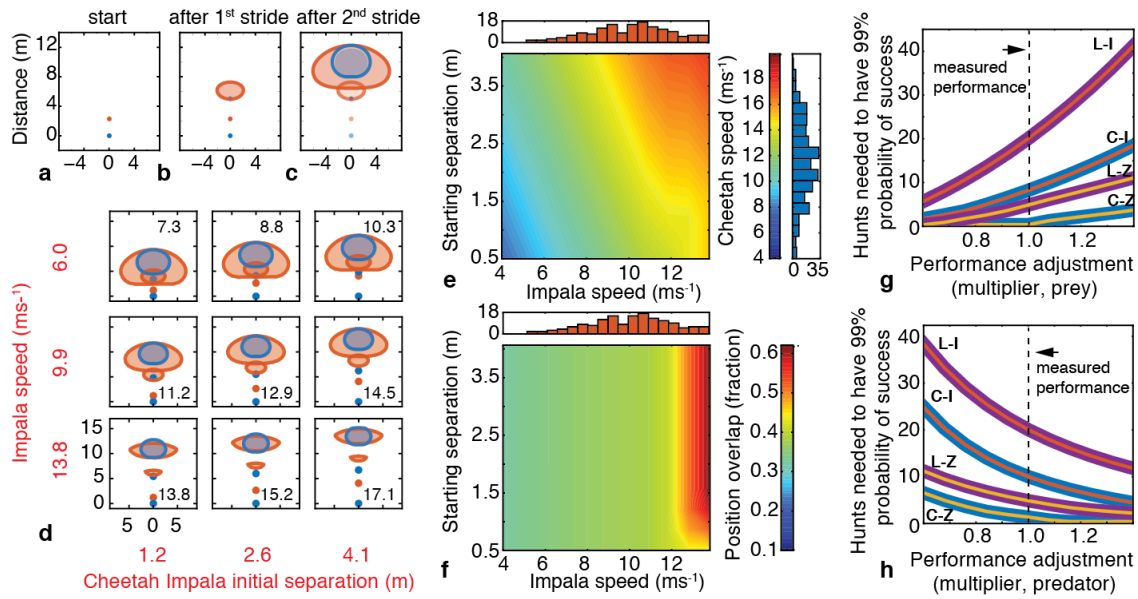
Figure 4. Output of model of predator prey interaction and impact of performance differential on hunt outcome. (a) Plot showing predator (blue) and prey (red) at start of simulation, both have initial velocity towards the top of the page and initial separation. **(b)** After one stride the prey can move to anywhere in the red ellipse by acceleration in the appropriate direction. Predator velocity unchanged since there is no prey acceleration in the previous stride to react to. Initial positions shown. **(c)** Red ellipse perimeter is the area prey can reach after two strides of chosen maximum acceleration. The blue-filled ellipse represents the locations the predator can occupy after its second stride (responding to the prey acceleration observed in first stride). The area of the prey ellipse that is covered by the predator ellipse line is defined as probability of capture. Predator is given a starting speed for each combination of prey speed and initial spacing which maximises the capture probability. Panel **(d)** show panel **(c)** for nine different cheetah-impala initial conditions, rows are different initial impala speeds, values in red to the left of each row. Columns are different initial predator-prey separations at the start of the simulation with values given in red below each column. Scale for all instances is given in the bottom left plot in meters in black. The inset black numbers in each sub-panel are the initial (optimised for maximum success) predator speeds in ms^{-1}. **(e)** the optimum cheetah speed to maximise overlap (hotter colours indicate faster speed, key on the right) as a function of impala speed (x axis) and starting separation (y axis). The histogram above the main plot shows the distribution of actual impala speed at first turn of 10 degrees or more for each run (same x axis as the main plot) and the vertical histogram shows distribution of actual cheetah speed at first turn (scale as for heat bar). **(f)** presents the proportional overlap (capture probability) as a function of impala initial speed and starting separation. **(g)** and **(h)** show the number of hunts required to have a 99% chance of prey capture for different performance levels of prey and predator. The maximum tangential and centripetal accelerations (but not speed) of the prey **(g)** or the predator **(h)** were multiplied by the x axis value and the simulation run at 8.75ms^{-1} initial prey speed and 2 m initial separation for all four combinations of predator and prey (dashed vertical line: actual performance measured). Labels give species pairings for each line and the inner colour is the prey and the outer colour the predator (colours as in Fig. 1).

12
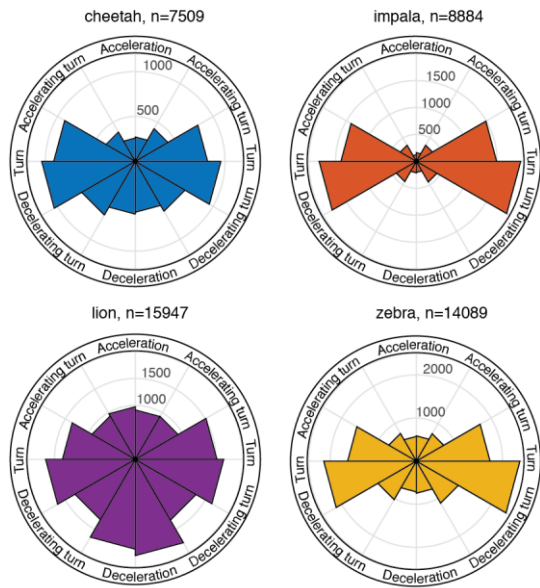
Figure 5. Orientation of direction of acceleration for each stride grouped by species. Circular histogram of frequency/direction of the acceleration vector for each stride (steady state strides removed) binned in twelve 30 degree sectors. Upwards is forwards acceleration, down is backwards, left and right are turning in that direction. Height of bin from centre is number of strides, scale on each plot. Stride numbers in figure.

13

Author Contributions: AW, TH, and TW conceived, designed and led the study, KG, JM, HB, EB organised field work, monitored animals and downloaded data. AW performed veterinary procedures, JL designed and built collars with input from AW. RD, ML, NC and TW undertook muscle experiments and interpreted the muscle data. TH, OD, TW and AW analysed data, SW created the model and undertook statistical analysis, AW wrote paper with input from all authors. The authors declare no competing financial interests.
Author Information: Reprints and permissions information is available. Correspondence and requests should be addressed to awilson@rvc.ac.uk.

Methods

Animals

All collared animals were located in northern Botswana with largely overlapping ranges (Fig. 1e). Animals were immobilised by free darting from a vehicle or helicopter mostly by AW, using **cheetah:** 80-100 mg ketamine 2 mg medetomidine; **lion:** 60 mg ketamine, 25 mg tiletamine hydrochloride, 25 mg zolazepam hydrochloride (as 50 mg zoletil, Virbac), 2mg butorphanol tartrate and 6 mg medetomidine; **impala:** 1.5 mg thiafentanil oxalate, 2 mg butorphanol tartrate and 1700 IU hyalase; **zebra:** 7 mg etorphine hydrochloride, 50 mg azaperone, 1700 IU hyalase. Herbivore reversal with diprenorphine or naltrexone, carnivores were reversed with atipamezole up to 60 minutes after darting. While sedated, front and hind leg and body lengths were recorded. Collar data were downloaded by radio link every few weeks to a ground vehicle and collars were monitored. All animals were adult, nine lion (two male, seven female), five cheetah (two male, three female), seven zebra (seven female), seven impala (six male, one female). The lion and cheetah were part of other ongoing projects in collaboration with the Botswana Predator Conservation Trust (http://www.bpctrust.org). Programmable drop offs (two models, 108 g, Sirtrack Ltd., Havelock North, New Zealand, collar independent power source or 50 g, Biotrack, Wareham, UK) were attached to the zebra and impala collars. Two drop-off units failed and collars were retrieved by re-darting. Data were collected between April 2012 - Nov 2016 (cheetah (June 2012 - April 2013), lion (April 2012 - June 2013), zebra (Nov 2014 - Sept 2015), impala (July - Nov 2016)). A subset of the cheetah data (367/520 runs) were analysed in[9].

Muscle fibre measurements

Biopsies were taken from the *biceps femoris* muscle by AW, using a Bergstrom needle or chonchotome forceps following collar placement. Animals were clipped, sterility ensured and the biopsy site treated with local antibiotics (200 mg cloxacillin, 75 mg ampicillin, Curaclox LC, Norbrook) and the animal given analgesia (Finadyne or Metacam). Five male impala killed for meat were dissected and provided additional muscle samples. Muscle samples were skinned by 30 min of immersion in ice-cold relaxing solution containing 2% Triton-X 100 and exposed to pH 6 relaxing solution to inactivate any foot-and-mouth disease virus. Triton was washed out with fresh relaxing solution and samples were immersed in 500 mM trehalose containing 0.5% glycerol[22] frozen in liquid nitrogen and stored in an IATA-approved dry-shipper (Biotrek 3' Statebourne Cryogenics, Washington, UK) for transport to the UK. In the UK, biopsies were stored at -80 °C. Periodically, individual biopsies were thawed and had cryopreserving trehalose replaced with a relaxing solution. Our previous work showed that biopsies stored for 20 months using this protocol showed no discernible loss of mechanical power[22]. Thawed biopsies were stored at -20 °C in a relaxing solution made up in glycerol and used for fibre preparation and testing within four weeks.

Fibre fragments were first suspended while in relaxing solution between the motor and force transducer of a 600A permeabilised fibre apparatus (Aurora Scientific, ON, Canada). T-shaped aluminium clips were attached to fibre ends and used to suspend fibres from steel wire hooks that were glued with shellac to the motor and transducer. Fibres were visualised using a 900B digital camera (Aurora Scientific, ON, Canada). The camera image was used to set

sarcomere length (*SL*) of a fibre fragment to between 2.5 and 2.6 μm. Fibre length (*L$_o$*), depth and width were then measured, in mm. Fibre cross-sectional area (CSA) was calculated for every fibre, assuming an elliptical shape.

Single skinned fibres were activated by temperature-jump (T-jump), from 1 °C to 25 °C (Extended Data Fig. 2a), using approaches similar to those previously described[22]. The composition and ionic strength (200 mM) of the various solutions was as previously described[22]. To activate a fibre, it was immersed successively through solutions for low-temperature pre-activation (for 45 s), low-temperature activation (for 4 s), high-temperature activation (6 s), and high-temperature relaxation. The example record in Extended Data Fig. 2a shows the time-courses of solution changes and force responses for an impala fibre, starting from the final 3 s of cold-temperature pre-activation. The force baseline at 0.7*L$_o$* was recorded in high-temperature relaxing solution before re-setting *L$_o$* to the original starting length and checking *SL*.

The standard procedure to measure fibre power and determine peak power was modified to perform four different force control events during each 6 s activation to deliver more data per fibre[22]. Briefly, after T-jump to 25 °C, force developed to a plateau at constant length (isometric force), and the fibre was then was clamped for 20 ms to a predetermined fraction of peak isometric force – the actual force achieved in the first force clamp was calculated by the 600A based on the difference between baseline force (measured and stored within a 600A protocol just prior to 1 °C activation) and isometric force (measured and stored within a 600A protocol just before onset of a force-clamp). The shortening velocity during force-clamp was measured and used to calculate power output. The fibre was then released to slack length in order to re-measure baseline force and it was then lengthened to *L$_o$* over a period of 5 ms. This avoids a high eccentric force transient during lengthening. The baseline measurement was saved again in the 600A protocol and used to compare with the measurement of stable isometric force achieved after lengthening the fibre to *L$_o$* – the force attained in the next force-clamp was based on the difference between the new saved values of baseline and isometric force. Four different force control events were conducted during each 6 s activation at 25 ℃ (see Extended Data Fig. 2a). Examples of a force clamp and of the fibre length changes required to hold force constant are shown in Extended Data Fig. 2b and 2c. Relaxation and a final force baseline-check were also conducted at 25 °C (Extended Data Fig. 2a). Three activations provided up to twelve different force-clamp measurements in order to quantify a normalised power *vs* force relationship and peak power for each fibre (see below).

A fibre was counted as 'tested' if it did not break on the test apparatus, and if test conditions (solution temperature and chemistry) were maintained as prescribed by the experimental design. A fibre was counted as 'included' in the mechanical tests if (i) the maximum isometric force > 75 kPa, and (ii) during the repeated activations, isometric force for each test remained > 80% of the peak isometric force observed. For each fibre, we conducted three activations, each with four force control, or shortening, events in order to collect maximally 12 points for a power-force curve-fit. An individual data point (i.e. a single force control event) could be rejected (either because of poor, e.g. unstable/oscillating, force during fibre-shortening or because of low (< 80% of max) isometric force), but exclusion of a data point on this basis will not necessarily have caused the fibre to have been rejected unless the spread of usable data points was insufficient for curve fitting. Of the 209 fibres initially tested with apparent

success, 35 were excluded (three of 40 cheetah fibres, 14 of 64 lion fibres, 14 of 71 zebra fibres, four of 34 impala fibres).

The data for each fibre were analysed as described previously[22], after normalising fibre force to the dimensionless F (force during shortening) / F_{isom} (isometric force) and normalising fibre power to Power (in Watts) / ($F_{isom} \cdot L_o$ in N and m, respectively) which has units of s^{-1}. The relationship between normalised power (called Q) and normalised force is described by a version of the Hill force-velocity equation:

$$Q = \frac{\left(\frac{Q_{max} \cdot F_o}{F_{Q_{max}}^2}\right) \cdot F \cdot \left(1 - \left(\frac{F}{F_o}\right)\right)}{1 + F \cdot \left(F_o - 2 \cdot F_{Q_{max}}\right)/F_{Q_{max}}^2} \qquad (1)$$

including terms for the force intercept (F_O on a plot of Q against $Force/F_{isom}$, force at peak power ($F_{Q_{max}}$), and maximum normalised power (Q_{max}). An example plot and best-fit curve is shown in Extended Data Fig. 2d. Peak power in units W kg^{-1} is obtained by multiplying Q_{max} by maximum isometric stress in units kPa and dividing by fibre density, 1.064 g ml^{-1} [38].

After mechanics tests, the 'low performing' single skinned fibres were pinned out onto a gelatine base in cryomolds, flooded with OCT (Tissue-Tek, Sakura Finetek USA), and frozen in liquid nitrogen. Sections (8 µm thick) were cut and immuno-stained with mouse anti-MHC fast monoclonal antibody [MY-32] (1:1000 ab51263, Abcam, Cambridge, UK) for type 2 fibres, and mouse anti-MHC slow monoclonal antibody (1:50 MAB1628, Merck Millipore, Burlington, USA) for type 1 fibres.

Muscle statistics

A linear mixed-effects model was fitted in R (R Foundation for Statistical Computing) for peak power, velocity at peak power, stress at peak power, and isometric stress against a factor distinguishing predator and prey with the interaction of this factor with a categorical variable 'performance classification'[39]. Within the factor distinguishing predator and prey, we included a nested random effect by subject and fibre. The residuals of this model exhibited heteroscedasticity and so the variance of the error term was allowed to vary by 'performance classification'. General linear hypothesis tests were then performed.

Temperature

This work was carried out at 25 ºC whereas most published studies were carried out at temperatures below 25 ºC. Muscle power is highly temperature-dependent[25] and West et al[26] consider their own and literature data and find that in the temperature range 20 to 35 ºC, a temperature coefficient (Q_{10}; ratiometric increase in rate with a temperature increase of 10 degrees) of 2.3 is appropriate[40,41] (see[26] Fig. 7). A Q_{10} of 2.3 was used to predict powers at a body temperature of 38 ºC.

Whole animal performance

The collars provided GPS position and instantaneous velocity data as well as three-axis-specific force, rotation rate and magnetic orientation data. To reduce noise, improve precision and increase temporal resolution in the position and velocity data, GPS and IMU measurements were fused[9] using a 12-state extended Kalman filter followed by a Rauch–

Tung– Striebel smoother written in MATLAB (The Mathworks Inc., MA, USA). Data were segmented into strides, and non-gallop strides removed, as described in[42] and locomotor parameters determined for each stride. Stride data were separated into non-uniform speed bins with 400 data points in each and the 98th percentile of value determined for each bin. End bins with fewer than 400 data points were ignored. This approach gives a value that represents regularly-used high performance locomotion, albeit one that is lower than the absolute maximum value recorded[9] and it excludes data from other less athletic hunting styles. The approach is robust to noise and occasional non-Gaussian outliers inherent in GPS derived data. For the polar acceleration plot (Fig. 3n) we combined left and right acceleration and separated the data into six bins so the number of points varied (Fig. 5). We also extracted the highest value for speed by species defined as the highest value achieved by three individuals.

Collar design
Collar design changed slightly over time and between species. The main change occurred between the predator and herbivore collars with a change of GPS unit, IMU unit and the addition of a second low-powered IMU but none of these had any significant impact on collar data/performance.

All collars were constructed in-house. The transparent top housing (holding the electronics) was either cast from polyurethane resin using a silicon mould and a rapid prototyped former (Aprocas GmbH, Barleben, Germany) or vacuum formed in-house (300XQ, Formech International Limited, Herts, England) from polycarbonate (4mm Clear Lexan Exell D, General Electric Company) over formers and assembled using two pack acrylic resin (Devweld 531, ITW Devcon, Danvers, USA). The design varied with the curvature of the neck for different species. A vacuum-formed, Kevlar tape reinforced 4mm polycarbonate battery box with lid holding the rechargeable and non-rechargeable batteries in potting compound (A6090 NP1480 Water Clear Polyurethane Potting Compound, ALH Systems, Wiltshire, UK) was mounted on the lower side of the collar belt, providing a counterweight to the top housing. Ethical guidelines suggest a collar mass limit of 5 -10% of body mass[43] to minimise the impact on the animal; our collars were below that threshold at 0.3 to 1.0% (collar mass: cheetah 340 g, lion 970 g, zebra 930 g + 108 g drop-off, impala 450 g + 50 g drop-off). The electronics package was similar in all collar versions with almost identical functionality.

The major challenge in recording high sample rate data in wildlife collars is to manage the energy consumption in order to maintain a sufficient collar life span. To enable collars to operate for long periods of time, the collars used solar cells and a rechargeable battery and dynamically switched between different sample rate modes depending on the animal's activity. The collar circuit was based around a low power MSP430 16-bit microcontroller (Texas Instruments Inc., Dallas, USA), running software written in the 'C' programming language developed using an integrated development system from IAR Systems. The microcontroller contains several internal peripheral blocks, including an 8-channel 12-bit analogue-to-digital converter (ADC), four serial communications modules, plus various timers, general-purpose digital input and output lines, and other support modules. A connected 2 GB micro-SD flash memory card (Sandisk Corp., Milpitas, USA) provided data

storage.

GPS position was obtained from an LEA-6T GPS module (u-Blox AG, Thalwil, Switzerland) in predator collars and from an NEO-6T or NEO-M8N GPS module (u-Blox AG) in herbivore collars. In addition to internally-computed position and velocity, the module is able to generate raw pseudo-range, phase and Doppler data for the signal from each satellite enabling detailed GPS performance evaluation, and use of customised differential techniques for increased accuracy.

The collar circuit also included an inertial measurement suite, based on MEMS (microelectromechanical systems) devices. In predator collars, acceleration was measured using an MMA7331 three-axis accelerometer module (Freescale Semiconductor, Inc., Austin, USA), providing acceleration with a ±12 g range. The roll and pitch rotation rate was measured by a dual-axis gyroscope LPR550AL (ST Microelectronics N.V., Geneva, Switzerland), and yaw rotation rate by a single-axis gyroscope LY550ALH (ST Microelectronics), both set to the 2,000 $°s^{-1}$ range. Sensor outputs were filtered by a simple single-pole analogue filter (100 Hz knee), and then sampled by the microcontroller at the ADC sample rates defined below. Originally 300 Hz was chosen for the accelerometer data (100 Hz for gyroscopes) as giving an overhead to a frequency of 30 Hz; that is, 1/minimum published stance time in cheetah[44]. In herbivore collars we used a combined accelerometer and gyroscope: MPU6050 (±16 g, ±2000 $°s^{-1}$, 250 Hz data in data streaming, 125 Hz data from accelerometer only during pre-trigger buffering); magnetometer: HMC5883 (15 Hz during data streaming, 7.5 Hz data during lower activity level profiles). A low-power accelerometer: MMA8652 (±8 g, was sampled at 50 Hz for activity logging and data stream triggering).

Collar data recording
The collars were able to switch between different operating states based on acceleration measurements and the chosen software configuration. Earlier collar versions, exclusively deployed on predators, were more power-hungry and a balance between high sample rate measurements and long-term ecological studies on specific individuals had to be found.

These collars had three main operating states, with time of day restrictions on high sample rates. Generally, if the animal was deemed to be stationary ('resting state') the sample rate was one GPS fix per hour; if the animal was moving slowly, ('mooch state') position was recorded at intervals that ranged between 60 s and 5 minutes (depending on the current configuration) and if the animal was deemed to be running, GPS sample rate was 5 Hz and IMU data (300 Hz, see above) were recorded simultaneously. High sample rate mode ('chase state') was often restricted to the main hunting times of the species during the day to avoid battery drainage due to potential false triggering outside those windows.

Animal activity was determined by the accelerometer and used to control operational states of the collar. In predator collars the accelerometer monitored activity at 30 Hz for a period of 10 s in every minute if the collar was in 'resting state'. Within each 10 s sampling period, the

peak-to-peak acceleration was computed for each axis every 2 s, and an accumulator incremented by a specified value for each 2 s window in which the peak-to-peak acceleration exceeded a pre-set threshold. For each 2 s window in which the peak-to-peak acceleration did not exceed the threshold, the accumulator was decremented by a (different) specified value. Thus, periods of movement could be given higher influence than periods of no movement or vice versa to identify stalking. If the accumulator total exceeded a specified value, the animal was deemed to be consistently moving and the collar switched to a higher operating state termed 'mooch state'. In 'mooch state' the accelerometer monitored activity constantly at 30 Hz and a similar algorithm with different weights and thresholds was then used to determine when the animal had settled back to rest. When consistently moving the GPS was refreshed every 30 s.

High sample rate recording ('running/chase state', 5 Hz GPS, 300 Hz accelerometer, 100 Hz gyroscope data) was triggered when the horizontal acceleration signal crossed a threshold deemed to be representative for running, provided it was in the 'slow moving state' and the event occurred during a time window that allowed the switch. A file was stored if five further peaks (strides) were detected. Recording continued as long as the threshold was surpassed at least once within a five second window. Extra overrun time of between 5 and 20 s was added at the end of each trial (to avoid early cut offs and to provide static data to aid open loop integration back through the data). Trigger thresholds were species-specific and optimised to avoid false triggers over the first few months of collar deployment. Originally, trigger thresholds were based on accelerometer signals measured for running domestic dogs and horses. Thresholds were increased if the original setting (chosen on the cautious side) produced an excessive number of false triggers (trials that cannot be considered as runs). The newer herbivore collars featured a combined accelerometer/gyroscope unit MPU6050 (InvenSense Inc., San Jose, California) (±16 g, 2,000 $°s^{-1}$). The change led to a reduction in the acceleration sample frequency from 300 Hz to 250 Hz (125 Hz for gyroscopes) in zebra collars. A 100 Hz digital filter internal to the MPU6050 was applied to the raw data. Power conservation considerations led to a further reduction to 50 Hz in impala collars (50 Hz for gyroscopes, digital filter 21 Hz). The change to 50 Hz was implemented after verifying that the lower sample rate did not lead to a detectable change in results. A separate low power 3-axis accelerometer unit MMA8653 (NXP Semiconductors N.V., Eindhoven, Netherlands) (±8 g) was added to constantly monitor the activity state of the animal at a sample rate of 50 Hz and to switch collars into a high sample rate state. 'Resting state' was eliminated in herbivore collars due to their inherently active lifestyle, reducing the number of operational states to two, 'slow moving' and 'running'. The switch to 'running state' was permitted at all times.

Collar performance
Cheetah collars (oldest collars) delivered a first fix in 1.3 s after triggering (median), accurate position data (<10 m s.d.) after 1.6 s, and full rate data (5 Hz) after 5.4 s. Impala collars (newest collars) showed a slight improvement with time to first fix being 1.1 s (median), accurate position data (<10 m s.d.) after 5.0 s, and full rate data (5 Hz) after 5.2 s.

A 2.4 GHz chirp-spread-spectrum communication module (Nanotron Technologies Gmbh, Berlin Germany) communicating at 1 Mbit per second was used to download data and upload software configurations and firmware updates. A conventional wildlife tracking transmitter in the 149 MHz band (Sirtrack, Havelock North, New Zealand or African Wildlife Tracking, Pretoria, South Africa) was used for long-range animal tracking using conventional direction-finding techniques from the ground or the air.

Power for the predator collars was provided by a single 13 Ah lithium thionyl chloride primary battery (Saft Groupe SA, Bagnolet, France) and a 900 mAh lithium-polymer rechargeable battery (Active Robots, Radstock, UK), charged by a solar cell array consisting of ten monocrystalline silicon solar cells (KXOB22-12X1, Ixys, Milpitas, USA). Zebra collars used two primary batteries and the impala collars used a smaller lithium polymer battery, (165 mAh, 3.7 V, LP-402025-IS-3,Shenzhen Bak Energy Co., Ltd, Shenzhen City, China).

Battery voltages and the charge current from the solar cell array were monitored by the microcontroller, which switched the collar's electrical load from one battery to the other depending on battery state. Average collar power consumption varied greatly depending on the collar version and the activity pattern of the species and the individuals. Solar cell power output also varied considerably depending on the species' sun exposure.

Signal processing
GPS–INS processing was used to reduce noise and improve precision in the position and velocity solution, as well as increasing the temporal resolution of the data. GPS and IMU measurements were fused using a 12-state extended Kalman filter[45] in loosely coupled architecture. The total state formulation used propagates position, velocity and orientation states with time using the IMU measurements in a simplified form of the strap-down inertial navigation equations[46]. The associated process noise was estimated from the known error characteristics of the inertial sensors used. GPS position and velocity updates were used as measurement updates, and receiver accuracy data for each fix used to estimate measurement noise to appropriately weight the GPS to the inertial solution.

The filter was run in reverse time from the last GPS observation of each run to the beginning of the buffered inertial data. During the short time period in which only inertial data was present (delay between trigger and first GPS fix), the filter propagation was equivalent to open-loop inertial navigation. The filter was initialised using last GPS position and velocity data, and Euler angles assumed zero with covariances appropriate for the uncertainty in that assumption. A Rauch-Tung-Striebel (RTS) smoother[47] was then applied in forward time on the Kalman filtered data. This is equivalent to combining backward and forward solutions, effectively halving the open-loop INS integration period between GPS observations. In cases when it was not possible to reconstruct the period before the first GPS observation (time too long or GPS accuracy insufficient), runs start at medium speeds rather than very low speeds.

Data analysis

Trials were Kalman filtered and only those that were filtered successfully, contained at least three strides, and stride speed (see cutting of strides below) exceeded 3 ms^{-1} were counted as true runs and analysed further using MATLAB (Mathworks Inc., MA, USA).

Calculation of speed and stride times

Vertical accelerations were used to determine stride times. A zero phase band pass Butterworth filter (4th order) was applied with cut-off frequencies of 1 Hz and 6.6 Hz (twice the maximum stride frequency in the cheetah and impala). A peak detection function was used to detect peaks with a minimum period of 0.25 seconds between peaks and a minimum peak height of 0.1 g.

Species-specific gait parameters such as transition speeds and expected stride frequencies for walking and trotting (based on[42]) were used to remove double peaks in strides in symmetrical gaits. Horizontal stride speed was derived from the Kalman filtered velocity averaged over strides in order to remove the effects of speed fluctuation through the stride and collar oscillation relative to the centre of mass.

Tangential acceleration, change of heading and centripetal acceleration over stride

Stride times were used to calculate tangential (fore-aft) acceleration, centripetal (turning) acceleration and change in heading between strides. The displacement vectors between consecutive strides were then calculated:

$$\overrightarrow{P_{i-1}P_i} = \vec{P_i} - \overrightarrow{P_{i-1}} \tag{2}$$

and

$$\overrightarrow{P_iP_{i+1}} = \overrightarrow{P_{i+1}} - \vec{P_i} \tag{3}$$

Where $\vec{P_i}$ is the two-dimensional position at sample/stride i.

Change of heading ($\Delta\theta_i$ was calculated from the angle between the two vectors:

$$\Delta\theta_i = sin^{-1}\left(\frac{\left|\overrightarrow{P_iP_{i+1}} \times \overrightarrow{P_{i-1}P_i}\right|}{\left\|\overrightarrow{P_iP_{i+1}}\right\|\left\|\overrightarrow{P_{i-1}P_i}\right\|}\right) \tag{4}$$

Angular velocity (ω_i was derived by dividing the change of heading by the time between mid-stride positions ΔT:

$$\omega_i = \frac{\Delta\theta_i}{\Delta T} \tag{5}$$

The tangential or fore-aft acceleration ($a_{t,i}$ and centripetal acceleration ($a_{c,i}$ were then computed from mid-stride speeds v_i :

$$a_{t,i} = \frac{v_{i+1} - v_i}{\Delta T} \tag{6}$$

$$a_{c,i} = \frac{v_i^2}{r_i} = \omega_i v_i \tag{7}$$

Negative values for tangential acceleration represent deceleration. Absolute values were used for centripetal acceleration, equalling right and left turns. For visual purposes the data in Fig. 3n were mirrored around the vertical axis.

Mass-specific centre of mass (COM) stride work (net COM kinetic energy change in a stride) was calculated as change in speed over a stride multiplied by stride average speed. Mass-specific COM power was calculated as the dot product of stride averaged tangential acceleration and stride averaged velocity (that is, multiply forward acceleration by forward speed):

$$P_{t,i} = a_{t,i} v_i \tag{8}$$

Calculation of grip limits

Grip limits are shown in Fig. 3. Friction poses a limit to acceleration and is the product of friction coefficient μ and force normal to the surface (based on acceleration due to gravity, g). Therefore the maximum total horizontal acceleration a_{max} is limited to:

$$a_{max} = \mu g \tag{9}$$

with a_{max} being the resultant (combination) of tangential and centripetal acceleration:

$$a_{c,max} = \mu g; a_{t,max} = \mu g; \tag{10}$$

Maximum turning speed v_{max} depends on friction, gravity and turning radius and is calculated based on equation (6,9):

$$v_{max} = \sqrt{\mu g r} \tag{11}$$

Calculation of stride frequency

Regression lines were fitted to stride frequency versus speed data at running speeds. Sections with running data were identified using an unsupervised clustering algorithm on three features derived from windows of accelerometer signals (4 s long)[42]. Features were chosen based on domain knowledge and were the standard deviation of the horizontal and vertical axis accelerometer signals and an autocorrelation estimate of the stride frequency[42]. Features were normalised to have zero mean and unit standard deviation before they were clustered using the k-means algorithm. The number of clusters was determined using the Davis-Bouldin criterion[48] and human inspection. Subsequently, the sections identified to contain running data were isolated and vertical acceleration was used to determine stride times (see above), stride frequency was calculated from the time between acceleration peaks. Regression lines were calculated for the subgroup from each bin representing the middle 60%, the highest 20% of positive and highest 20% of negative power (Fig. 3b,g).

Maximum performance analysis

Extracting values that reflect maximum performance carries the risk of choosing outliers generated by non-Gaussian GPS noise rather than realistic values. Previous work reduced the risk of overestimating performance by weighting stride parameters such as stride speed and accelerations by the previous and following stride[9,37,49]. Here we chose a different approach, not weighting but calculating the 98th percentile for each of a number of bins (Fig. 3) in order

to also address the impact of different sample sizes and accelerations that were not sustained for three consecutive strides. In addition, obvious errors (speeds >30 ms^{-1} and total stride averaged accelerations of $>\pm20$ ms^{-2}) were removed from the dataset.

An inherent issue with comparing the performance of different species lies in their different movement patterns, with lion and zebra having a considerably higher proportion of straight, constant low speed strides than impala and cheetah. In order to extract manoeuvring strides, a cut-off based on the magnitude of the total horizontal acceleration (combined tangential and centripetal acceleration) was performed. This cut-off could not be universal because different animals had different amounts of low speed steady state behaviour in their accelerometer traces. This manifested itself in large differences between species in kurtosis of the acceleration distribution histograms. To address these differences a species specific cut-off was used. To ensure that this cut-off still gave comparable results for the different species the characteristic scale of the kurtosis for each distribution was estimated via:

$$s_\alpha = \sigma_\alpha k_\alpha^{\frac{1}{4}}$$ (12)

where s_α is our characteristic scale, σ_α is the standard deviation and k_α is the Pearson's kurtosis, all for species α. If a cut-off of c_α was used for one species then we can calculate the cut off for species β via:

$$c_\beta = \frac{s_\beta}{s_\alpha} c_\alpha$$ (13)

The effect of this cut off on the distribution of total horizontal acceleration is shown in Extended Data Fig. 3a,b.

In Fig. 3n tangential acceleration is plotted versus centripetal accelerations. The Cartesian coordinates were transformed into polar coordinates in order to bin the data. Calculations were performed on absolute centripetal acceleration values to boost data point numbers in bins and then mirrored on the vertical axis; the semicircle was divided into a total of 6 bins.

The cut-off was adjusted so that the number of data points in a bin was at least 200 for all species. The cut-off was determined by the impala, which had the lowest number of data points.

The parameters were plotted versus horizontal speed (except for stride frequency) and the 98th percentile was calculated for each of a number of speed bins whose width was defined by the requirement to include 400 data points. The final (highest speed) bins with less than 400 data points were discounted. In Fig. 3 a moving average of 3 bins was applied to all data except Fig. 3n. Data were interpolated to allow the calculation of species performance ratios (Fig. 3) at 1 ms^{-1} speed positions.

Statistical analysis

The maximum performance of the predator and prey were compared using a set of linear models of maximum positive and negative power, positive and negative tangential acceleration and absolute centripetal acceleration.

The maximum performance of each individual was quantified by taking the 98th percentile of the positive and negative tangential acceleration and absolute centripetal acceleration of each individual.

Negative and positive power covaried with speed and were binned by speed as above and the 98th percentile within each bin computed for each subject within a species. A linear regression was then performed and the predicted power at 8 ms^{-1} calculated for each subject.
Linear models were fitted to these data using restricted maximum likelihood, with the maximum powers and accelerations as dependent variables, against a factor for predator *vs* prey and a factor for each pairing (zero for cheetah-impala and one for zebra-lion). Models with an interaction term between these two factors were fitted but comparing these models to those previously described (this time fitted using maximum likelihood) indicated the interaction term was superfluous (effect sizes were small and associated p-values not significant). The interaction term was therefore dropped from the analysis in all models, except when comparing stride frequencies where there was a substantial interaction term (effect sizes large and associated p-values significant). Here the model was fitted by individual species.
Due to the presence of heteroscedasticity the error term was allowed to vary by species. Identical models were fitted modelling stride frequency, but with the predator-prey term replaced with a species term due to detectable and manifest across species differences.

Chase-evasion model

The model combines the observed acceleration capacity with a maximum speed constraint to produce possible position profiles for predators and prey in the subsequent two strides of a chase. We simulate the possible positions of the prey given the prey's initial speed. We then do the same for the predator, optimising the predator's initial speed to give maximum overlap in final positions of the predator and prey.

We begin with the observed maximum accelerations for our subjects (Extended Data Table 3b). We approximate the possible impulsive accelerations of the animals by assuming they have a maximum tangential acceleration forward, *at*, a maximum reverse tangential acceleration *atr*, and a maximum centripetal acceleration *ac*. The profile of possible accelerations is assumed to be two half-ellipses with the semi-minor axis along the direction of motion. The top ellipse has semi-minor axis radius *at*, the bottom ellipse has semi-minor axis radius *atr,* and both have a semi-major axis of length *ac*.

The animals are assumed to have a maximum possible speed, *v*. This places a further constraint on the possible profile of accelerations as no acceleration can result in a speed above this maximum.

To find this constraint we assume that a predator and its prey are galloping at a common stride frequency (Fig. 3b,g) and phase, and that the bulk of the impulse they can achieve in a stride is performed in a short duration (stance). On any given stride the animal can apply an impulse to change direction, subject to the constraint that the resulting speed cannot be greater than the animal's maximum speed, *vM*. If the animal is at a speed *v* along a unit direction $\hat{t}$ and an impulsive acceleration $a_0\hat{t} + a_1\hat{t}$ with $\hat{f}$ perpendicular to $\hat{t}$ is to be applied then the resulting speed is:

$$\left(v + \frac{a_0}{f}\right)^2 + \left(\frac{a_1}{f}\right)^2 \qquad (14)$$

where f is the stride frequency. This must be less than vM. This implies a pair of quadratic relations between $a0$ and $a1$ subject to v and vM of the form:

$$a_0 = \pm\sqrt{(v_M^2 - v^2)f^2 - a_1^2 - 2a_1 vf} \qquad (15)$$

The simulation allows our subjects to accelerate to anywhere within the area formed by the union of the area above the negative root of this equation, below the positive root, and within the two half ellipses previously mentioned.

We note that the possible acceleration profile depends both on the position of the animal and its current speed (an animal that is slow will not be constrained by its maximum possible speed, while one going at its maximum speed cannot accelerate forward). This means that simulating the animal's possible positions forward in time increases in complexity with each stride taken, as both the new position of the animal and the new speed must be retained. As such we confined ourselves to simulating two strides forward from our starting conditions; that is, we are only concerned with strategies for the predator and prey at the very end of a chase.

We assume that the prey performs an evasive acceleration on the first stride, while the predator continues to chase without changing velocity. On the second stride the prey again accelerates, and now the predator also has the ability to react to the acceleration it observes in the first stride. We ran 100 such simulations for starting separations varying from the maximal separation that makes capture possible within two strides down to half a predator length separation (cheetah=0.66 m[50], lion=0.92 m[51]). If the prey and predator are closer than this, then the predator is already close enough for prey capture.

For a given prey speed and initial predator-prey separation we find the predator speed which maximises the capture probability by means of a Nelder-Mead simplex optimisation, subject to the constraint that the initial predator speed must be greater than or equal to the initial prey speeds. Due to ambiguity in the solution space, a small penalty term encouraging faster speeds from the predator was added in the form $eps*v_{pred}$, with $eps=10^{-6}$. This ensured that where there was a range of optimal 'best speeds' for the predator the fastest was selected. This had no impact on the value of the optima up to four significant digits.
In order to test how a change in predator or prey performance influences hunt outcome, we adjusted the performance by multiplying the maximum recorded tangential and the centripetal accelerations of the prey or predator by a number ranging from 0.6 to 1.4 to deliver values to insert into the model for animals of greater or lesser athleticism respectively. This number is the x-axis performance adjustment in Fig. 4g,h and rerunning the simulation to obtain capture probabilities. Maximum speed was not changed.

Code availability

Python code for this simulation Predator-Prey Model and data are available as Source Data files.

Data availability

The authors declare that all relevant (processed not raw) data supporting the findings of this study are available as two Source Data files. Any further data are available from the corresponding author upon reasonable request.

List of symbols

i, stride number; $\vec{P_i}$, two-dimensional position; $\Delta\theta_i$, signed change of heading; ω_i, heading angular velocity; ΔT, sampling interval; a, total horizontal acceleration; at, tangential or forward acceleration, $a$tr tangential reverse acceleration; ac, centripetal acceleration, a_0 and a_1 are generic accelerations; r, turn radius; v, stride averaged horizontal speed, v_{max}, maximal turning speed, vM, maximum speed; P_t, mass-specific fore-aft power; μ, coefficient of friction; m, body mass; g, gravity. α, β, species indices; s characteristic scale; σ standard deviation; k is the Pearson's kurtosis.

References

38   Méndez, J. & Keys, A. Density and composition of mammalian muscle. *Metabolism* **9**, 184-188 (1960).
39   Pinheiro, J. & Bates., D. *Mixed-effects models in S and S-PLUS.* (Springer, 2000).
40   Ranatunga, K. Temperature dependence of mechanical power output in mammalian (rat) skeletal muscle. *Exp. Physiol.* **83**, 371-376 (1998).
41   Barclay, C., Woledge, R. & Curtin, N. Is the efficiency of mammalian (mouse) skeletal muscle temperature dependent? *J. Physiol.* **588**, 3819-3831 (2010).
42   Dewhirst, O. P. *et al.* An exploratory clustering approach for extracting stride parameters from tracking collars on free ranging wild animals. *J. Exp. Biol.*, jeb. 146035 (2016).
43   Sikes, R. S. *et al.* 2016 Guidelines of the American Society of Mammalogists for the use of wild mammals in research and education. *J. Mammal.* **97**, 663-688 (2016).
44   Hudson, P. E., Corr, S. A. & Wilson, A. M. High speed galloping in the cheetah (*Acinonyx jubatus*) and the racing greyhound (*Canis familiaris*): spatio-temporal and kinetic characteristics. *J. Exp. Biol.* **215**, 2425-2434 (2012).
45   Kalman, R. E. A new approach to linear filtering and prediction problems. *J. Basic. Eng.* **82**, 35-45 (1960).
46   Titterton, D. & Weston, J. L. *Strapdown inertial navigation technology*. 2 edn, Vol. 207 (AIAA, 2004).
47   Rauch, H. E., Striebel, C. & Tung, F. Maximum likelihood estimates of linear dynamic systems. *AIAA journal* **3**, 1445-1450 (1965).
48   Davies, D. L. & Bouldin, D. W. A cluster separation measure. *EEE Trans. Pattern Anal. Mach. Intell.*, 224-227 (1979).
49   Hubel, T. Y. *et al.* Additive opportunistic capture explains group hunting benefits in African wild dogs. *Nat. Commun.* **7**, doi:10.1038/ncomms11033 (2016).

50   Estes, R. D. The behaviour guide to African mammals: including hoofed mammals, carnivores, primates. *Johannesburg: Russell Friedman Books CC* (1991).

51   Nowak, R. M. *Walker's mammals of the world*. Vol. 1 (JHU Press, 1999).
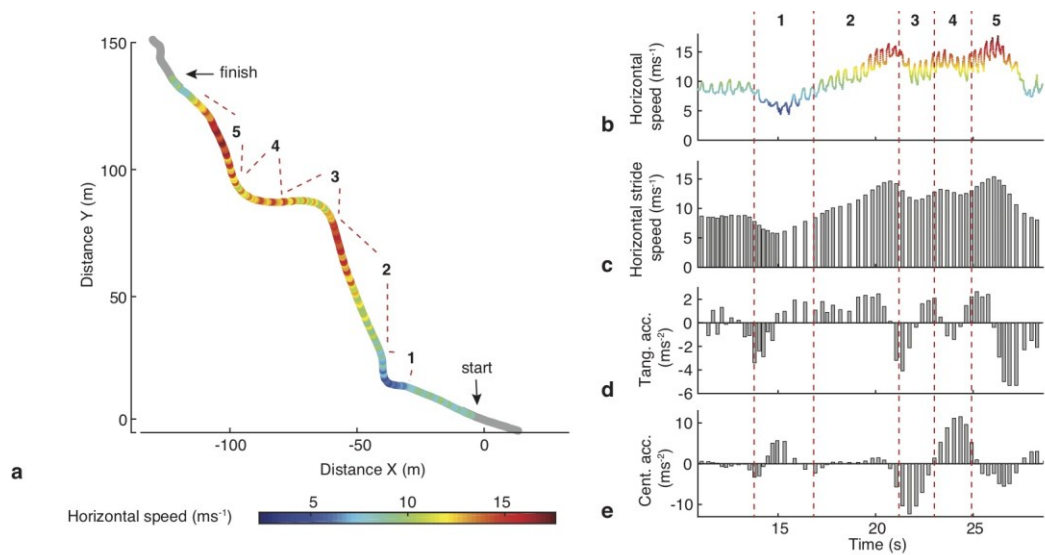
| Species	Number of individuals	Number of trials	Total strides	Strides used (non-steady state)	Number of strides per run (mean±s.d)	Distance per run (m) (mean±s.d.)
Cheetah	5	520	23871	7509	50 ± 25	157 ± 122
Impala	7	515	22491	8884	47 ± 33	151 ± 149
Lion	9	2726	101110	15947	39 ± 22	80 ± 76
Zebra	7	1801	64952	14089	38 ± 39	69 ± 91

f

Extended Data Figure 1 | GPS data summary. (a) example manoeuvring sequence for a cheetah showing position based on fused GPS-IMU data (250 Hz) colour-coded according to speed and segmented for clarity (1-5, duplicated in (b-e)), **(b)** speed based on fused GPS-IMU data (250 Hz) **(c-e)** stride-wise values for speed (averaged over stride), tangential (fore-aft) acceleration (change in stride speed/stride durations) and centripetal (lateral) acceleration ((change in heading/stride duration)*stride speed). **(f)** Table showing details of animals used and data sets collected. Reduced dataset of non-steady state stride used for analysis of maximum performance. Note: Number of strides and distance per run based on all strides (steady state included).
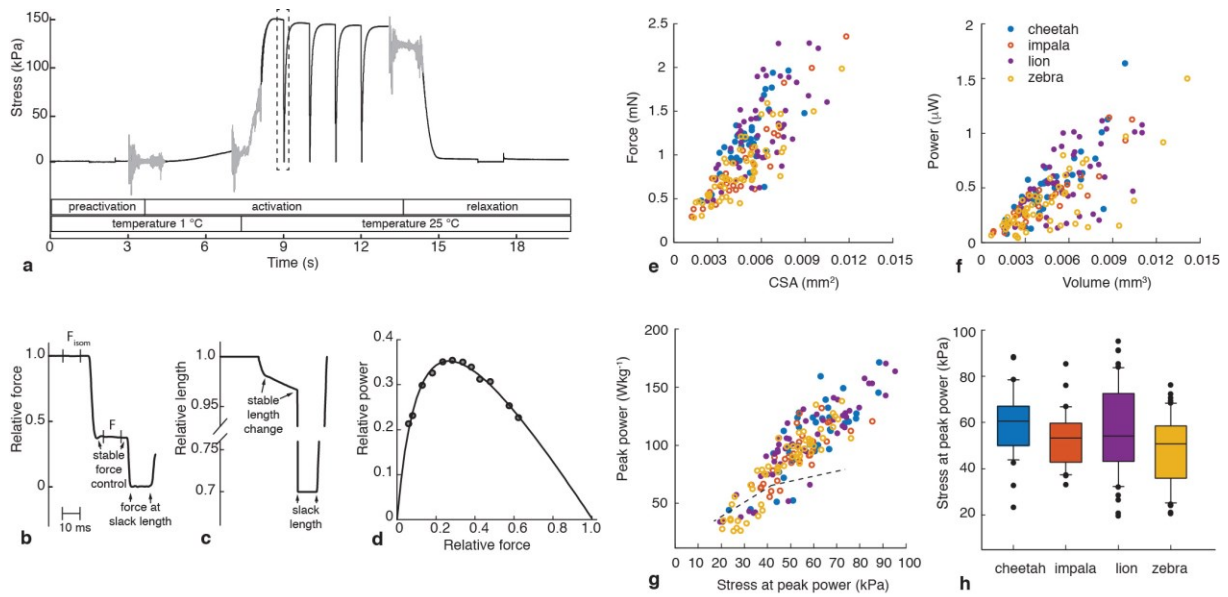
| | n | Isometric stress (kPa) | Peak power (Wkg^{-1}) | At peak power | |
				Velocity (L_os^{-1})	Stress (kPa)
Cheetah	37	237.7 ± 7.5	101.6 ± 5.2	1.81 ± 0.06	59.2 ± 2.3
Lion	50	220.0 ± 8.6	96.6 ± 5.3	1.80 ± 0.05	56.2 ± 2.7
Both predators	87	227.5 ± 5.9	98.8 ± 3.7	1.80 ± 0.04	57.5 ± 1.8
High performing fibres only (predators)	76	234.1 ± 6.2	107.9 ± 3.1	1.91 ± 0.03	60.5 ± 1.8
Impala	30	194.9 ± 7.7	84.8 ± 4.3	1.69 ± 0.05	52.9 ± 2.3
Zebra	57	192.1 ± 6.1	75.2 ± 4.3	1.62 ± 0.05	47.3 ± 2.0
Both prey	87	193.1 ± 5.1	78.5 ± 3.2	1.64 ± 0.04	49.3 ± 1.5
High performing fibres only (prey)	72	201.4 ± 5.1	88.7 ± 2.5	1.78 ± 0.03	53.1 ± 1.4

Extended Data Figure 2 | Muscle data summary. **(a-c)** Time course of stress (force) development in a single skinned impala fibre, showing transition of the fibre through pre-activation, activation and relaxation solutions, and stress development after temperature-jump (T-jump) from 1 to 25°C. The sample rate was 5 kHz. The grey noisy parts of the stress trace denote periods of solution-change. The four downward 'spikes' in the stress record (at 9, 10, 11 and 12 s) are distinct periods of 'force control', where the fibre length was first rapidly reduced from L_o and then reduced at an appropriate rate to maintain force at pre-defined sub-maximal levels. The broken-line box in **(a)** surrounds the first episode of force control and is presented in **(b)** and **(c)** on an expanded time scale. **(b)** Relative force, F(force during shortening)/F_{isom}(isometric force), was reduced to 40% of maximum for 20 ms. Isometric force (F_{isom}) and the force during force clamp (F) were recorded as average values for the central 10 ms intervals (vertical lines). A force measurement F_{isom} was recorded just prior to each of the four force control events and used in the calculation of F/F_{isom}. Shortening speed (units L_o s^{-1}) was derived from the rate of change in fibre length during each force clamp **(c)**. At the end of the force clamp, fibre length was 'quick-released' to a slack length (70% of L_o), where force reduced to the zero baseline. After 10 ms at slack length, the motor lengthened the fibre back to the starting length (L_o), isometric stress was re-established (as shown in (a)) and another force control event was initiated. Twelve points on a power-force relationship **(d)** could be obtained from three T-jump activations of a single fibre. The curves were fitted (see Methods for more details) to give normalised power (Power/$F_{isom}L_o$, units s^{-1}) as a function of relative force (F/F_{isom}). The normalisation of both variables is important in the curve-fitting process chiefly because the measurements of F_{isom} often vary between and within activations; in the example shown (a) there was a small reduction in F_{isom} through the activation at 25ºC. **(e)** Peak isometric force relative to fibre cross-sectional area (CSA) for fibres from the four species. **(f)** Power output relative to fibre volume. There was a distinct subpopulation of 'low performance' fibres (mostly from lion and zebra) that displayed lower power at a given fibre volume. Fibres with a shortening velocity at peak power of < 1.35 lengths s^{-1} (see also Figure 2c) were classified as low performance. **(g)** Peak power relative to stress at peak power. The low performers also had stress at peak power values that were relatively low - the data points below the thin dashed black line have velocities of shortening < 1.35 MLs^{-1}. The variability in stress at peak power **(h)** was similar across the species tested. **(i)** Table showing details of muscle fibres. Mean (± SEM) mechanical features for single skinned skeletal muscle fibres from biceps femoris of cheetah, lion, impala

and zebra. Mean values are also categorised for the predator and prey groups, and further as the 'high performing' sub-groups of fibres (high performing fibres had optimal shortening speeds > 1.35 ML s^{-1}, see text and supplemental figures).
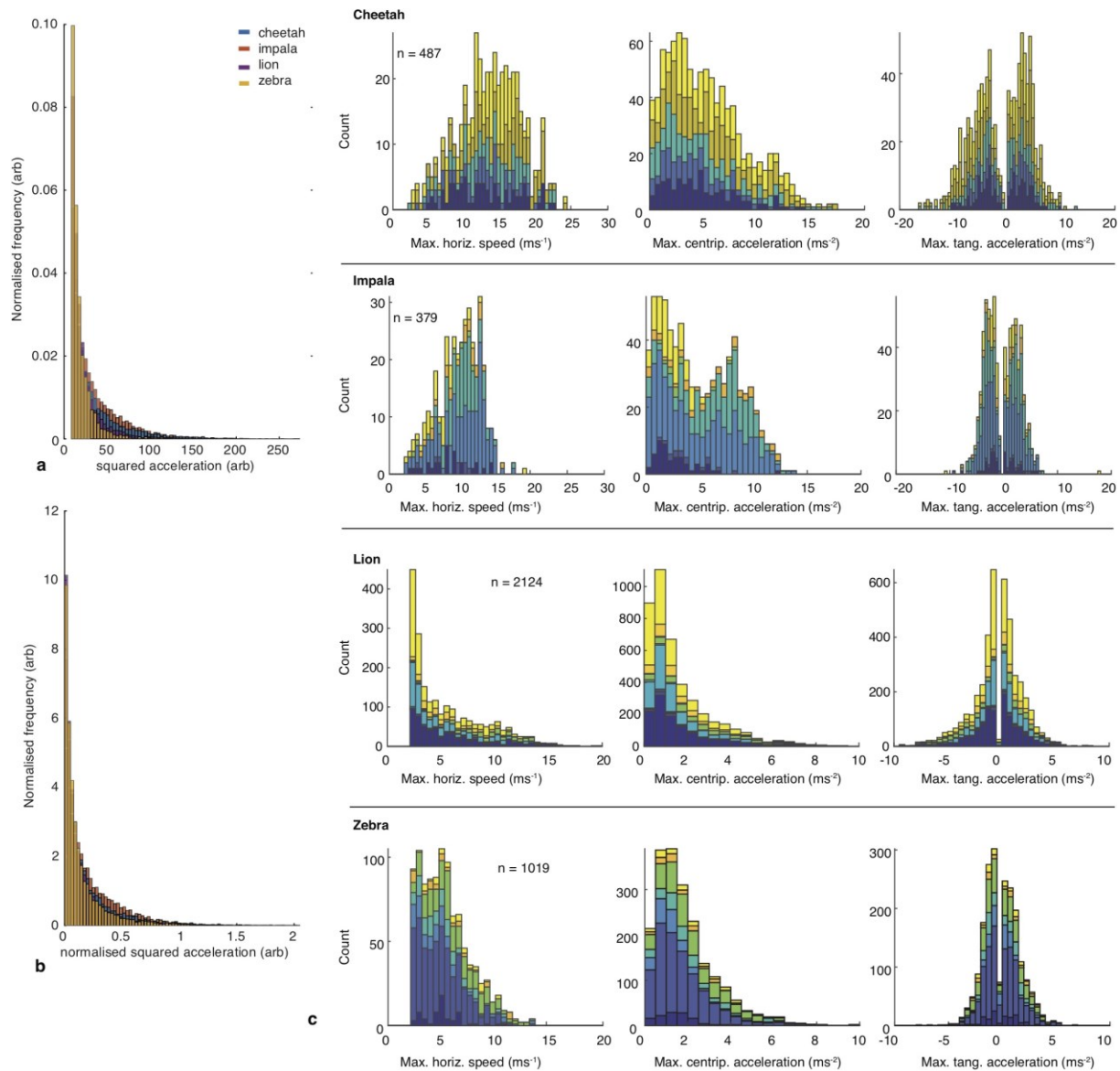
**Extended Data Figure 3 | Predator prey run comparisons**. Histograms of all strides **(a)** and extracted non-steady state strides **(b)**, where the cut off was species-specific based on their kurtosis. The x-axis is the normalised and squared horizontal acceleration (ie combined tangential and centripetal), in **(b)** on the x axis the cut-off is zero and the 98th percentile is one. Species color-coded cheetah (blue), impala (red), lion (lilac), zebra (yellow). This figure demonstrates the effect of removing steady state strides in delivering a similar distribution tail for all four species. This is critical for the 98th percentile being equally representative in all four species. **(c)** Histogram of maximum stride parameters recorded in each run (speed, centripetal and tangential acceleration) for each species. Color-coded by individuals, n: number of runs used for data extraction. One concern of the comparison between predator and prey species is the potential lack of high performance runs in prey species due to the low number of actual one on one chases. However, the distribution of the performance data shows that the cheetah and impala data include a considerably higher proportion of high performance runs while the lion and zebra dataset includes a large percentage of slower runs. Recognising that the species differ in run characteristics (motivation, proportion of steady state vs non steady state strides) we removed steady state strides, based on the species specific kurtosis, resulting in a comparable distribution in all four species (see methods).
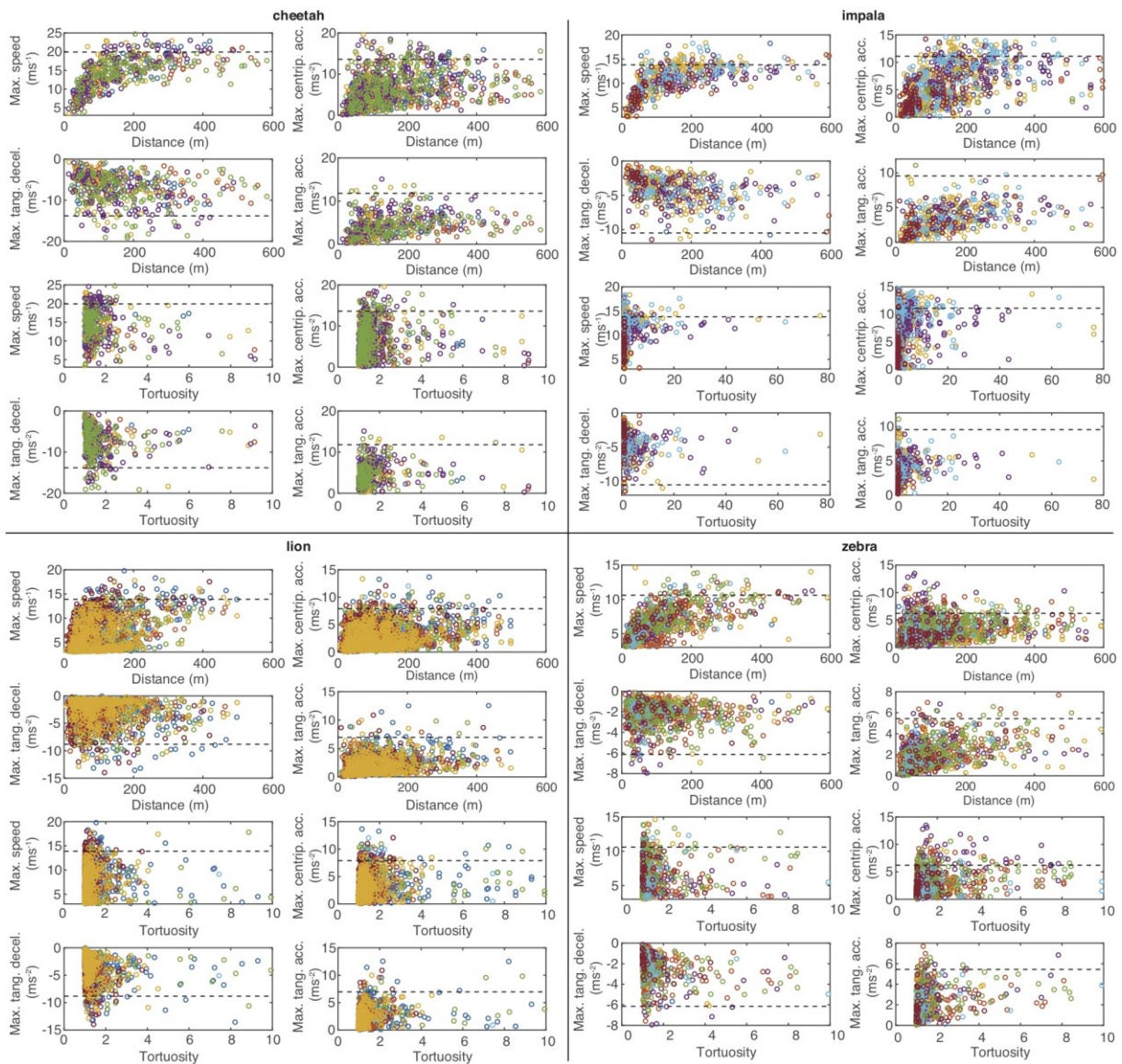
Extended Data Figure 4 | Maximum accelerations and speeds were extracted from each run and displayed versus distance covered during the run and versus tortuosity of the run. Tortuosity is the ratio of distance covered in a run to net displacement (distance between start and end of the run). Markers color-coded by individual, dashed black line maximum values based on 98th percentile. Number of runs (data points) are given in Extended Data Figure 1f, Cheetah, 520, Impala, 515, Lion, 2726, Zebra 1801.
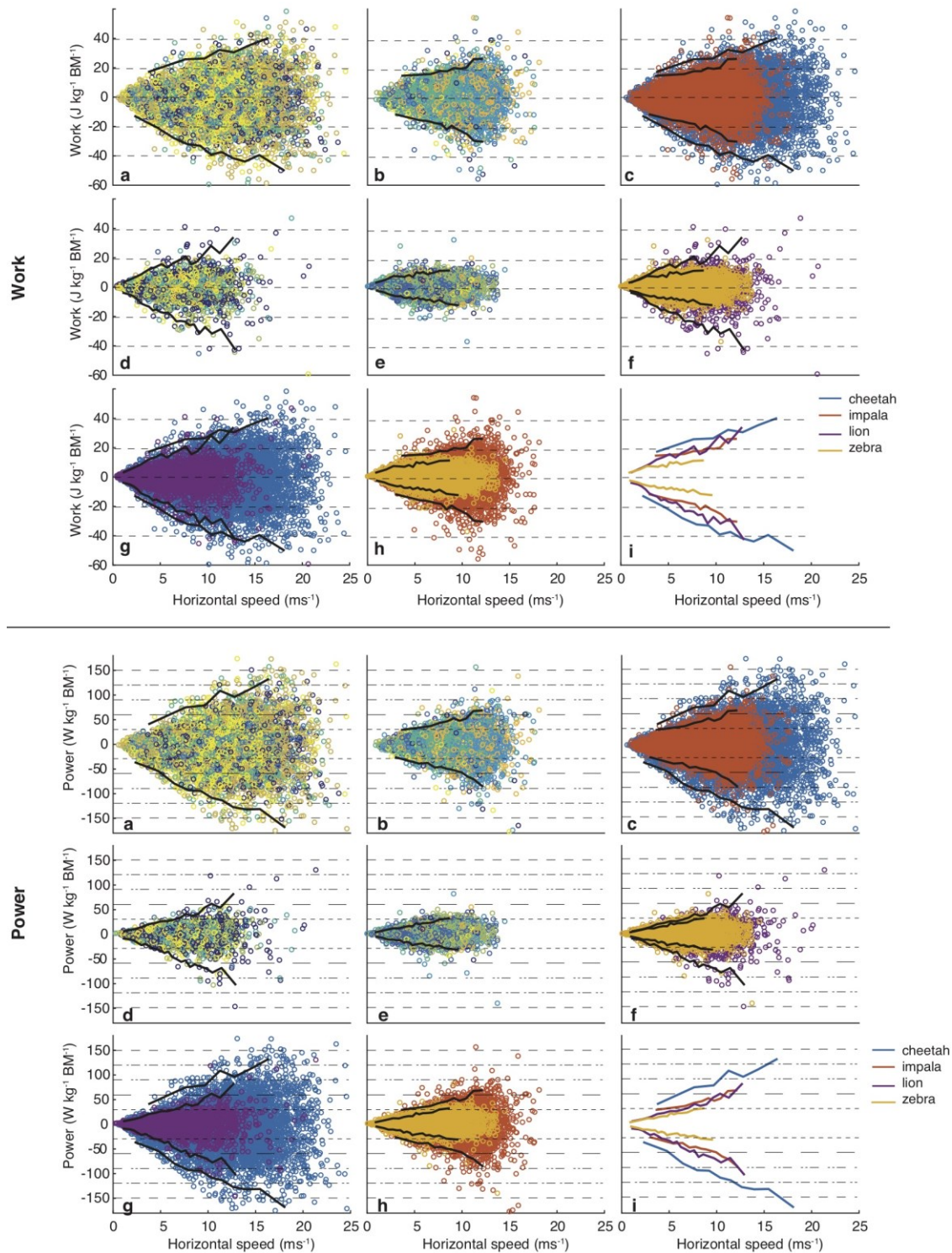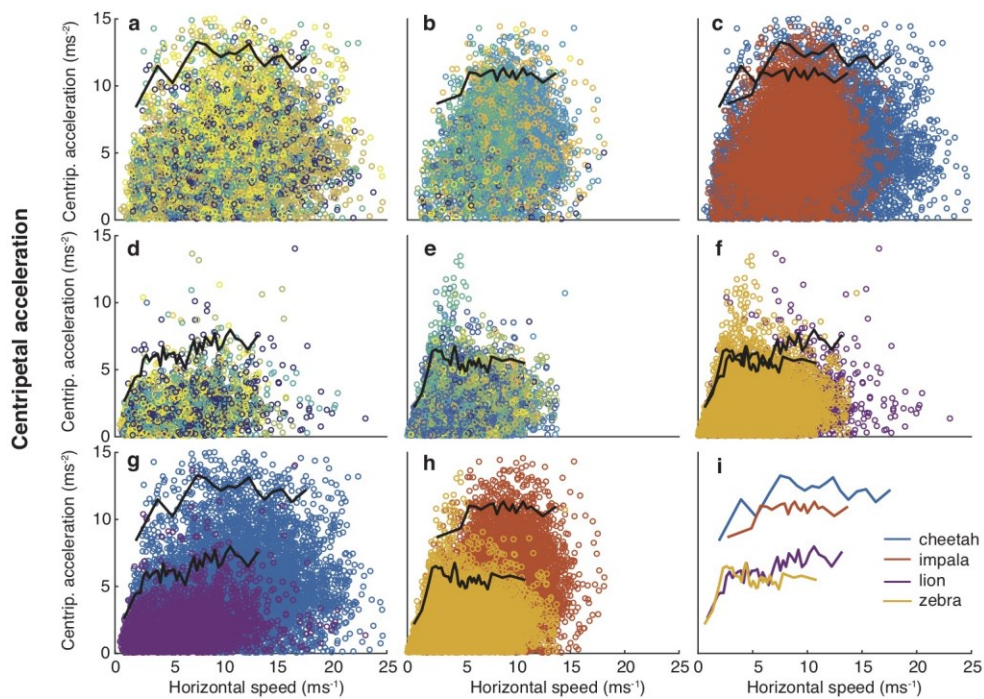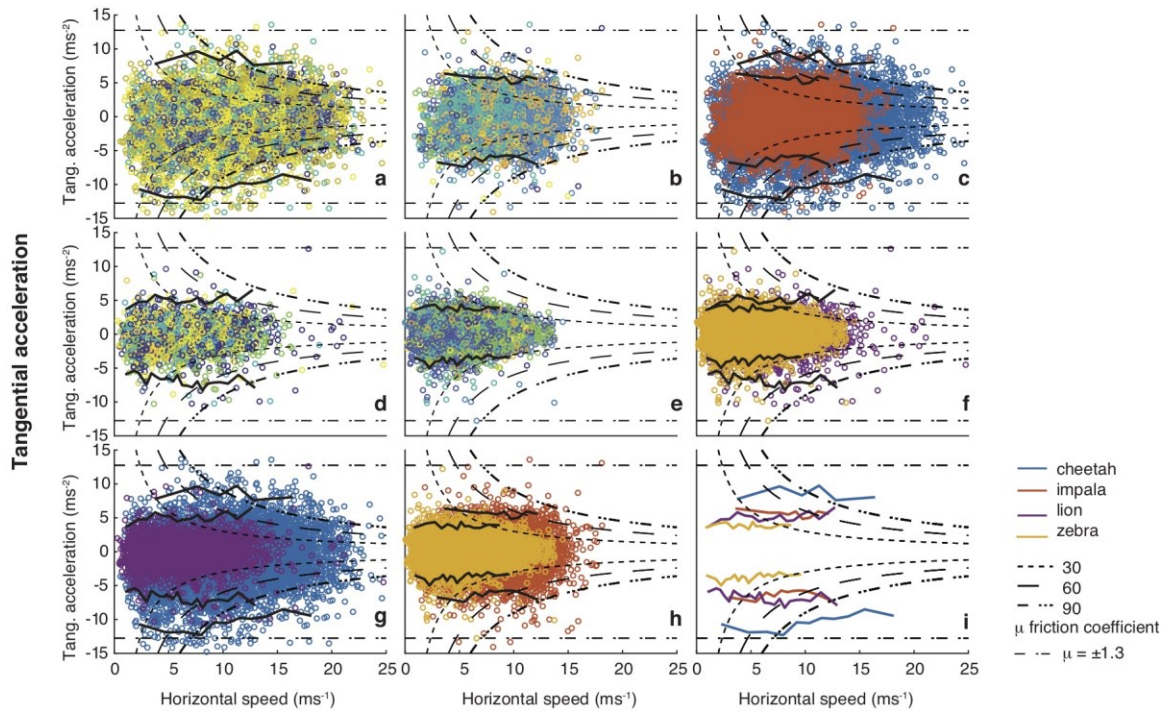
Extended Data Figure 5 | Work and Power analysed for each species. (a) cheetah; **(b)** impala; **(d)** lion; **(e)** zebra including the data points and line demarcating the 98th percentile for data in speed bins as represented in Figure 3 (a,b,d,e) Markers color-coded by individual, solid black line: 98th percentile. **(c,f,g,h)** Comparison of the predator prey pairs **(c)** cheetah-impala, **(f)** lion-zebra, and the predator and herbivore species **(g)** lion-cheetah, **(h)** impala-zebra, **(i)** shows the 98th percentile for all four species. (c,f,g,h,i) color-coded by species (legend in (i)).

In all four species maximum negative power was similar to maximum positive power. Muscle stress can be considerably higher when performing negative work than positive work[1,2] and a 60% higher fascicle power in lengthening (rather than shortening) has been reported[2], so mass-specific muscle power can be much higher in deceleration[3]. Body geometry relative to the ground reaction force vector or grip may limit the attainable horizontal ground reaction force[4] and the muscles need to be arranged to lengthen whilst experiencing the large

horizontal forces. Many of the propulsive muscles are hip retractors (Extended Data Table 2) which are not configured to resist forward motion).

1	Lindstedt, S., LaStayo, P. & Reich, T. When active muscles lengthen: properties and consequences of eccentric contractions. *Physiology* **16**, 256-261 (2001).
2	Roberts, T. J. & Azizi, E. The series-elastic shock absorber: tendons attenuate muscle power during eccentric actions. *J. Appl. Physiol.* **109**, 396-404 (2010).
3	Abbott, B., Bigland, B. & Ritchie, J. The physiological cost of negative work. *J. Physiol.* **117**, 380-390 (1952).
4	Williams, S. B., Tan, H., Usherwood, J. R. & Wilson, A. M. Pitch then power: limitations to acceleration in quadrupeds. *Biol. Lett.* **5**, 610-613 (2009).

Extended Data Figure 6 | Tangential and centripetal acceleration analysed for each species. (a) cheetah; (**b**) impala; (**d**) lion; (**e**) zebra including the data points and line demarcating the 98th percentile for data in speed bins as represented in Figure 3 (a,b,d,e) Markers color-coded by individual, solid black line: 98th percentile. (**c,f,g,h**) Comparison of the predator prey pairs (**c**) cheetah-impala, (**f**) lion-zebra, and the predator and herbivore species (**g**) lion-cheetah, (**h**) impala-zebra, (**i**) the 98th percentile for all four species. **c, f-i**, Data are colour-coded by species (key is shown in **i**).
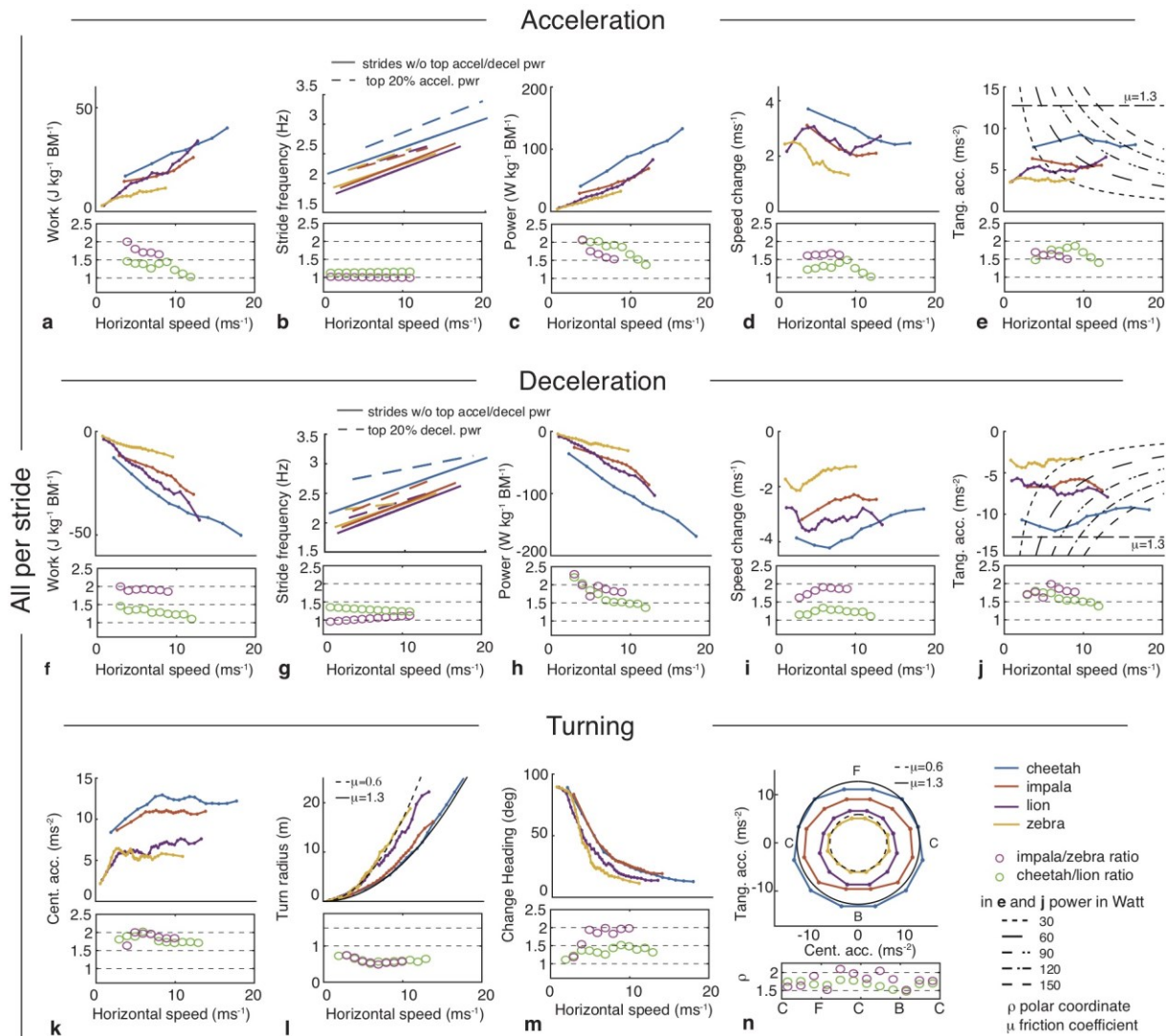
Extended Data Figure 7 | Locomotor performance based on stride parameters. This is the same as Figure 3 but the ratios compare the two predators and the two prey species. All values are averaged per stride or represent the change over a stride. Acceleration: **(a)** positive net work performed in each stride, **(b)** stride frequency **(c)** stride power **(d)** increase in speed per stride and **(e)** forward acceleration with the curved lines representing a mean power of 30, 60, 90, 120, 150 Watts. Parts **(f–j)** are the same figures as **(a-e)** but for decelerating strides. Turning: centripetal acceleration is presented in **(k)**, the relationship between speed and turn radius in **(l)** with limit lines for a coefficient of friction (μ) of 0.6 and 1.3, change in heading vs speed in **(m)** and lateral against tangential acceleration in **(n)** with limits as for μ. In **(n)** F represents pure forward acceleration, B deceleration and C acceleration to the side. In each panel there is one line per species which represents the 98th percentile for data in speed bins (bins always include 400 data points consequently bin width varies). cheetah – blue, impala – red, lion – purple and zebra – yellow. On the lower part of each panel the ratio of that parameter for cheetah to lion (green circle) and impala to zebra (magenta circle) is given for each speed bin.
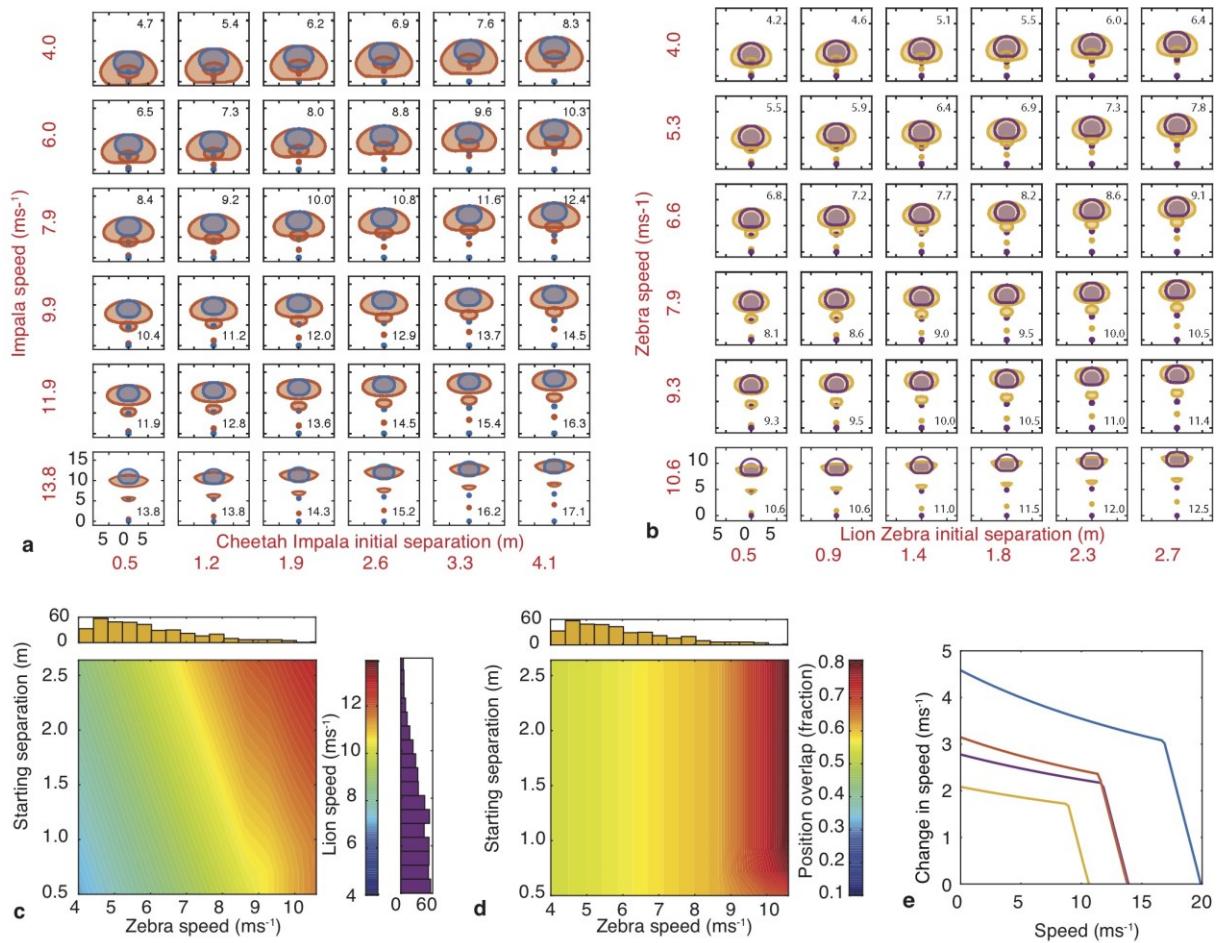
Extended Data Figure 8 |. Output of model of predator prey interaction and impact of performance differential on hunt outcome, see figure 4 for fuller explanation. (a,b) Plot showing output of simulation, Panels (a) and (b) are equivalent of Figure 4d with more subplots for cheetah-impala and lion-zebra respectively. At start of simulation, both have initial velocity towards the top of the page and initial separation. After one stride the prey can move to anywhere in the red/yellow ellipse by acceleration in the appropriate direction. Predator velocity unchanged since there is no prey acceleration in the previous stride to react to. Initial positions shown. Larger Red/yellow ellipse perimeter is the area prey can reach after two strides of chosen maximum acceleration. The blue/purple filled ellipse represents the locations the predator can occupy after its second stride (responding to the prey acceleration observed in first stride). The area of the prey ellipse that is covered by the predator ellipse line is defined as probability of capture. Predator is given a starting speed for each combination of prey speed and initial spacing which maximises the capture probability. Rows are different initial prey speeds, values in red to the left of each row. Columns are different initial predator-prey separations at the start of the simulation with values given in red below each column. Scale for all instances is given in the bottom left plot in meters in black. The inset black numbers in each sub-panel are the initial (optimised for maximum success) predator speeds in ms^{-1}. **(c)** the optimum lion speed to maximise overlap (hotter colours indicate faster speed, key on the right) as a function of zebra speed (x axis) and starting separation (y axis). The histogram above the main plot shows the distribution of actual zebra speed at first turn of 10 degrees or more for each run (same x axis as the main plot) and the vertical histogram shows distribution of actual lion speed at first turn (scale as for heat bar). **(d)** presents the proportional overlap (capture probability), as a function of zebra initial speed and starting separation. **(e)** shows modelled capacity for forward acceleration (speed increase per stride) as a function of speed (Extended Data Table 2b), cheetah – blue, impala – red, lion – purple and zebra – yellow.

Species	n	Provenance	Animal mass (kg)	Hind leg muscle	Front leg muscle	Spine/back muscle	Total locomotor muscle
Greyhound[51,52]	7 front 6 hind	R R	31.8	18.80%	18.40%	---	---
Greyhound[53]	9	R	27.3	---	---	9.70%	---
Cheetah[54,55]	8	Z	33.1	18.30%	14.20%	---	---
Impala	5	W	49.7	17.50%	11.30%	---	---
Horse[56]	7	D	510	19.40%	---	---	---
Horse[57]	6	D	503	---	6.60%	---	---
Arabian horse[58]	6	D	383	10.20%*	---	---	---
Quarterhorse[58]	6	D	457	12.70%*	---	---	---
Hare[59,60]	8	W	3.45	16.30%	9.30%	8.90%	34.50%
Ostrich[61]	11	F	105	33.70%	---	---	---
Ostrich[62]	2	F	100	30.29%	---	---	---
Lion[63,64]	1	Z	133	12.48%	14.30%	---	---
Beef Cattle[65]	---	F	544.3	28.00%	8.60%	---	---
Domestic Cat[66]	---	D	3.25	14.00%	---	---	---
Mix-Breed Dog[67]	1	D	23	10.40%	---	---	---

Extended Data Table 1 | Proportion of animal that is locomotor muscle. Data are taken from published values for athletic species and number of animals dissected given when reported. Provenance: wild (W), racing/competition (R), zoo (Z), farmed (F), domestic (D). Complete datasets including all muscles and the animal mass are sparse and many of the ones summarised are from our own group. In some of the studies the animals would be sedentary or have died from other causes so it is likely wild animals may have more muscle[18]. Gunn[19] reports that skeletal muscle as a fraction of body mass is 53% for Thoroughbred racehorses and 44% for other horses.

All values for muscle from both limbs as a percentage of total body mass. *Only 11 muscles reported.

References (Extended Data Table 1)
1. Williams S.B., Wilson A.M., Rhodes L., Andrews J., Payne R.C. Functional anatomy and muscle moment arms of the pelvic limb of an elite sprinting athlete: the racing greyhound (Canis familiaris). *J Anat.* **213**, 361–372 (2008).
2. Williams S.B., Wilson A.M., Daynes J., Peckham K., Payne, R.C. Functional anatomy and muscle moment arms of the thoracic limb of an elite sprinting athlete: the racing greyhound (Canis familiaris). *J Anat.* **213**, 373–382 (2008).
3. Webster E.L., Hudson P.E., Channon S.B. Comparative functional anatomy of the epaxial musculature of dogs (Canis familiaris) bred for sprinting vs. fighting. *J. Anat.* **225**, 317-327 (2014).
4. Hudson, P.E. et al. Functional anatomy of the cheetah (Acinonyx jubatus) forelimb. *J. Anat.* **218**, 375–385 (2011).
5. Hudson, P E. et al. Functional anatomy of the cheetah (Acinonyx jubatus) hindlimb. *J. Anat.* **218**, 363–374 (2011).
6. Payne R.C., Hutchinson J.R., Robilliard J.J., Smith N.C., Wilson A.M. Functional specialisation of pelvic limb anatomy in horses (Equus caballus). *J.Anat.* **206**, 557-574 (2005).
7. Payne R.C., Veenman P., Wilson A.M. The role of the extrinsic thoracic limb muscles in equine locomotion. *J. Anat.* **205**, 479-490 (2004).
8. Crook, T.C. et al. Comparative anatomy and muscle architecture of selected hind limb muscles in the Quarter Horse and Arab. *J.Anat.* **212**, 144-152 (2008).
9. Williams, S.B., Payne, R.C., Wilson, A.M. Functional specialisation of the pelvic limb of the hare (Lepus europeus). *J.Anat.* **210**, 472-490 (2007).
10. Williams, S.B., Wilson, A.M., Payne, R.C. Functional specialisation of the thoracic limb of the hare (Lepus europeus). *J.Anat.* **210**, 491-505 (2007).
11. Smith N.C., Wilson A.M., Jespers K.J., Payne, R.C. Muscle architecture and functional anatomy of the

pelvic limb of the ostrich (Struthio camelus). *J Anat.* **209**, 765–779 (2006).

12. Schaller, N.U. Structural attributes contributing to locomotor performance in the ostrich (Doctoral dissertation). Retrieved from archiv.ub.uni-heidelberg.de/volltextserver/8852/1/Schaller_Dis.pdf (2008).

13. Cuff A.R. et al. The scaling of postcranial muscles in cats (Felidae) II: hindlimb and lumbosacral muscles. *J. Anat.* **229** 142-152 (2016).

14. Cuff A.R. et al. The scaling of postcranial muscles in cats (Felidae) II: forelimb, cervical, and thoracic muscles. *J. Anat.* **229** 128-141 (2016).

15. Holland, R., Loveday, D., Ferguson, K. How Much Meat to Expect from a Beef Carcass. Retrieved from http://www.ansc.purdue.edu/SP/TBC/Documents/PB1822.pdf.

16. Sacks R.D., Roy, R.R. Architecture of the hind limb muscles of cats: functional significance. *J. Morphol.* **173**, 185-195 (1982).

17. Shahar, R., Milgram, J. Morphometric and anatomic study of the hind limb of a dog. *Am. J. Vet. Res.* **62**, 928-933 (2001).

18. Wilson, A. M. *et al.* Locomotion dynamics of hunting in wild cheetahs. *Nature* **498**, 185-189, 2013

19. Gunn, HM Muscle, bone and fat proportions and muscle distribution of Thoroughbreds and other horses. ICEEP 2 Proceedings, 253-264

Performance parameter	Predator	Herbivore
Pos. tangential acceleration (ms^{-2})	-0.5	-0.21
Neg. tangential acceleration (ms^{-2})	-0.42	-0.28
Pos. work (Jkg^{-1}BM^{-1})	-0.17	-0.45
Neg. work (Jkg^{-1}BM^{-1})	0.16	0.48
Pos. power (Wkg^{-1}BM^{-1})	-0.47	-0.41
Neg. power (Wkg^{-1}BM^{-1})	0.5	0.55

a

Species	Speed (ms^{-1})	Centrip. accel (ms^{-2})	Pos. tang. accel (ms^{-2})	Neg. tang. accel (ms^{-2})	Pos. work (Jkg^{-1}BM)	Neg. work (Jkg^{-1}BM)	Pos. power (Wkg^{-1}BM)	Neg. power (Wkg^{-1}BM)
Cheetah	19.9	12.3	8.3	-10.6	33.3	-39	109	-114
Impala	13.8	10.9	5.7	-6.3	22.1	-24	59	-60
Lion	13.9	6.5	5.2	-7	20.5	-24	48	-56
Zebra	10.6	5.6	3.9	-3.8	9.9	-9	24	-22

b

Extended Data Table 2 | Performance parameters. (a) Table showing Log-log slope of performance parameter vs mass for the two herbivore species and the two predator species. Stride values were extracted to represent species' performance and evaluated versus body mass to explore if the performance difference between small and large was concomitant with effects reported across a broad animal size range[1]. Parameters with increasing values (positive and negative work and power) were represented by maximum values while for parameters which plateaued (positive and negative tangential acceleration, centripetal acceleration) an average value was calculated. The slope of the logarithmic coordinates (log-log slope of performance parameter vs mass) was calculated for the two predators and two herbivores, respectively. The relationship is generally consistent in predators and in prey, with most parameters dropping with increasing size, but this does not provide an explanation for the magnitude of the differences seen since most parameters would scale weakly with animal size.

(b) Maximum (98%) values for stride parameters for all species. Maximum values were determined using the 98th percentile (after species specific steady state stride were removed from data, positive and negative data calculated separately). These are the parameters used in the model.

1. Alexander, R. M. *Principles of animal locomotion*, Princeton University Press, 2003